Extracellular Matrix Regulates Neuronal Chloride Concentration via K+-Cl−-Cotransporter 2

Tushar Devanand Yelhekar,[1] Tatiana Kuznetsova,[1,2] Evgenya Malinina,[1] Evgeni Ponimaskin,[2] Alexander Dityatev,[3,4,5] Michael Druzin,[1,*] and Staffan Johansson[1,*]

[1]Department of Integrative Medical Biology, Umeå University, SE-901 87 Umeå, Sweden

[2]Cellular Neurophysiology, Hannover Medical School, D-30625 Hannover, Germany

[3]Molecular Neuroplasticity, German Center for Neurodegenerative Diseases (DZNE), D-39120 Magdeburg, Germany

[4]Medical Faculty, Otto-von-Güricke University, D-39120 Magdeburg, Germany

[5]Center for Behavioral Brain Sciences (CBBS), Magdeburg, Germany

Abbreviated title: Extracellular matrix, neuronal chloride and KCC2

[*]Correspondence: Michael Druzin, Department of Integrative Medical Biology, Umeå University, SE-901 87 Umeå, Sweden; E-mail: michael.druzin@umu.se

or

Staffan Johansson, Department of Integrative Medical Biology, Umeå University, SE-901 87 Umeå, Sweden; E-mail: staffan.o.johansson@umu.se

Conflict of Interest: The authors declare no competing financial interests.

Abstract

The neuronal intracellular chloride concentration $[Cl^-]_i$ is critical for γ-aminobutyric acid type A (GABA$_A$) receptor-mediated transmission. Degradation of the extracellular matrix (ECM) is associated with raised $[Cl^-]_i$ but neither the mechanisms underlying this effect nor the consequences for GABA-mediated transmission are well understood. Hitherto it has been unclear how to reconcile the effect of the ECM on $[Cl^-]_i$ with the established role of cation-chloride cotransporters in setting $[Cl^-]_i$. In the present work we clarify the role of the ECM in the control of neuronal $[Cl^-]_i$. By measuring $[Cl^-]_i$ in central neurons from male rats we show that the ECM affects basal $[Cl^-]_i$ as well as the rate of Cl^- extrusion after a high load. The mechanism is not via impermeant anions but through regulation of K^+-Cl^--cotransporter 2 (KCC2). ECM degradation is accompanied by an N-type Ca^{2+}-channel- and calpain-dependent reduction in the amount of KCC2 protein, increased basal $[Cl^-]_i$, reduced Cl^- extrusion capacity as well as by reduced inhibitory, or even an excitatory, effect of intense GABA$_A$-receptor mediated trans mission. This implies a previously unrecognized pathway for the control of neuronal $[Cl^-]_i$ and excitability by the ECM.

Graphical abstract
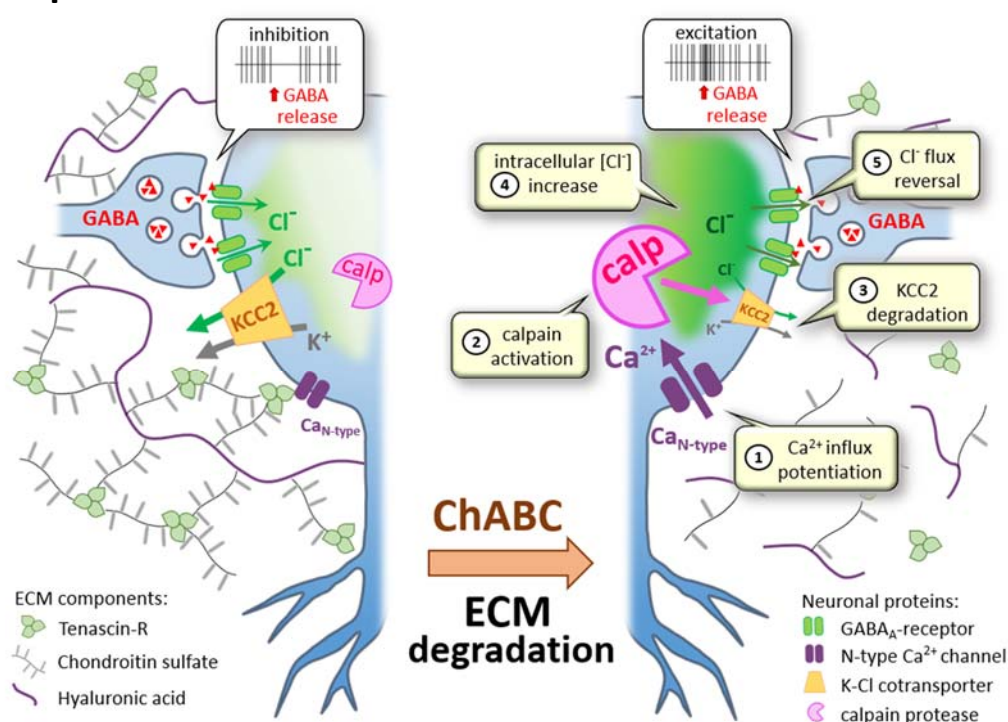
Keywords

43    $GABA_A$-mediated signalling

44   Extracellular matrix degradation

45   K^+-Cl^--cotransporter 2 regulation

Introduction

47    $GABA_A$ receptor-mediated neurotransmission is critical for normal brain function. The $GABA_A$

48   receptor-channel is permeable to Cl^- and thus the effect of activation depends critically on the

49   intracellular Cl^- concentration ($[Cl^-]_i$). The inhibitory action of $GABA_A$ receptors on neuronal

50   excitability that predominates in the adult brain is a consequence of a low $[Cl^-]_i$ (often 5 – 10 mM).

51   Higher $[Cl^-]_i$ is found early in development (Ben-Ari, 2002), in some adult neurons (Choi et al., 2008;

52   DeFazio et al., 2002; Haam et al., 2012) and in pathological conditions such as epilepsy (Huberfeld et

53   al., 2007) and chronic pain (Coull et al., 2003) and may be associated with an excitatory effect of

54    $GABA_A$-receptor activation. The extracellular matrix (ECM), which plays important roles in synaptic

55   plasticity and is proteolytically degraded during epileptogenesis (Soleman et al., 2013; Senkov et al.,

56   2014), may also be important for the control of basal $[Cl^-]_i$. Thus, it has been shown that ECM

57   degradation is associated with increased $[Cl^-]_i$ (Glykys et al., 2014a). The mechanism first suggested

58   to explain this effect involved negative charges maintained by the ECM (Glykys et al., 2014a).

59   However, the proposal questioned the previously ascribed role of the cation-chloride cotransporters,

60   Na^+-K^+-Cl^--cotransporter 1 (NKCC1) and K^+-Cl^--cotransporter 2 (KCC2) and has been questioned and

61   remains controversial (Ben-Ari, 2014; Cho, 2014; Delpire and Staley, 2014; Glykys et al., 2014b; Kaila

62   et al., 2014; Luhmann et al., 2014; Voipio et al., 2014; Savtchenko et al., 2017). NKCC1 and KCC2

63   remain seen as the main controllers of $[Cl^-]_i$. While NKCC1, if present, transports Cl^- into the cell,

64   KCC2 transports Cl^- mainly out of the cell, but may contribute to inward Cl^- transport depending on

65   the driving force set by the concentration of transported ions. KCC2 has been thought necessary to

66   maintain the low $[Cl^-]_i$ required for the common type of hyperpolarizing responses, including

67   inhibitory post-synaptic potentials, to GABA and glycine observed in mature central neurons (Kaila et

68   al., 2014). The question how the ECM affects $[Cl^-]_i$ and determines the inhibitory/excitatory effect of

69   GABA$_A$-receptor activation has remained unanswered.

70   In the present work, we analyze the mechanism by which the ECM influences $[Cl^-]_i$ and how it affects

71   GABA$_A$-receptor mediated transmission and neuronal excitability. By estimating $[Cl^-]_i$ directly from

72   electrophysiological recordings of Cl^- currents, we show that the integrity of the ECM is important for

73   the basal $[Cl^-]_i$ and also that the ECM strongly influences the rate of Cl^- extrusion after a high Cl^- load.

74   Our results, however, are not compatible with a mechanism involving a strong effect of negative

75   charges of the ECM (Glykys et al., 2014a). Rather, our combined electrophysiological and biochemical

76   results show that degradation of the ECM alters the amount of KCC2 via Ca^{2+} influx through N-type

77   channels and calpain activation, thus regulating the rate of KCC2-mediated Cl^- extrusion. Thereby the

78   ECM exerts an influence on the postsynaptic effects mediated by GABA$_A$-receptor activation and

79   preserves an inhibitory action in the presence of intense neuronal activity.

80   ## Materials and Methods

81   *Ethical approval*

82   Ethical approval of the procedures described was given either by the regional ethics committee for

83   animal research ("Umeå djurförsöksetiska nämnd", approvals no. A18-11 and A9-14) or by the

84   Hannover Medical School Institutional Animal Care and Research Advisory Committee, with all

85   experiments permitted by the local government (#33.14 42502-04-12/0753).

86   *Brain slice preparation*

87   Male Sprague-Dawley rats, aged 3 – 5 weeks, were used for the experiments. The procedures to

88   prepare 200 – 300 μm thick coronal brain slices containing the preoptic area have been described

89   elsewhere (Karlsson et al., 2011, modified after Malinina et al., 2005).

90   *Chondroitinase ABC treatment*

91   In some of the brain slices used, degradation of ECM was induced by chondroitinase ABC treatment

92   (ChABC) (0.2 U ml^{-1}; AMS Biotechnology) for at least 2 h at about 36 ^{o}C. ChABC was dissolved in

93   standard extracellular solution containing 0.1 % bovine serum albumin (BSA; Sigma-Aldrich). This

94   protocol for ChABC treatment has proved functional for slice preparations of brain tissue (Bukalo et

95   al., 2001; Hayani et al., 2018). The lower concentration of ChABC compared to that used e. g. by

96   Glykys et al. (2014a) is likely of advantage for minimizing possible non-specific side effects.

97   Histochemical verification of ECM degradation was performed as described below. Control slices

98   were exposed to similar treatment without ChABC. In some experiments, additional test substances,

99   as specified below, were present during ChABC exposure.

100   *Histochemistry*

101   Brain slices were divided in two cerebral hemispheres, for control and ChABC treatment (see above),

102   respectively. The most lateral part of cerebral cortex in ChABC-treated hemisections were cut off for

103   identification. After treatment, slices were fixed overnight in 4 % formaldehyde in phosphate-

104   buffered saline (PBS; Sigma-Aldrich). Following wash in PBS, slices were incubated in PBS-based

105   cryoprotectant solutions: 2×10 min in 10 % sucrose (w/v), 2×20 min in 20 % sucrose with 6 %

106   glycerol, then 2×30 min in 30 % sucrose and 12 % glycerol. Subsequently, the sections were carefully

107   placed in envelopes of aluminium foil for permeabilization of cell membranes by rapid freeze–thaw

108   cycles (Hughes et al., 2000). The slices were frozen by placement close above liquid nitrogen for 45 s

109   and thawed until all resulting condensation on the aluminium had disappeared. This freeze–thaw

110   cycle was repeated three times for each slice. After permeabilization, slices were rinsed three times

111   in 0.25 % BSA in PBS for 20 min each and then incubated in PBS containing 5.0 % BSA and 0.2 %

5

112   Triton X-100 (Sigma-Aldrich) for 1 h. Subsequently, slices were incubated with biotinylated *Wisteria*

113   *floribunda* agglutinin (WFA; 1:400; Sigma-Aldrich), diluted in PBS containing 2.5 % BSA. For negative

114   control slices, WFA was omitted. After incubation for 3 days at 4°C at a shaking platform, slices were

115   rinsed three to five times in PBS and exposed to streptavidin-Alexa 488 (1:300; Thermo Fisher)

116   overnight at 4°C. After three washes, slices were embedded in Vectashield mounting medium with

117   4',6-diamidino-2-phenylindole (DAPI; Vector Laboratories). Paired hemisections from ChABC-treated

118   and control groups were incubated together in one well, both in primary and in secondary reagent

119   mixtures, and mounted together under one cover slip.

120   For an overall view of slices and to estimate the effect of ChABC on WFA reactivity (Howell et al.,

121   2015; Morita et al., 2010), we used a conventional upright fluorescence microscope (Nikon Eclipse

122   80i) with a DS-U2 digital camera. Images were acquired with a 1.6× air objective using FITC (GFP)

123   filter (Ext 482/25, EM 530/40) for visualization of chondroitin sulphate proteoglycans, stained by

124   WFA. The exposure time for each filter was constant to enable comparison of signals in control and

125   experimental groups. The background fluorescence (average intensity in the negative control slice)

126   was subtracted from each image. To obtain images of full hemisections, separate images of

127   neighboring regions were acquired with overlap and then stitched using MosaicJ plugin of the Fiji

128   software.

129   To view perineuronal nets (PNNs) in control sections (as a positive control for WFA staining; Härtig et

130   al., 1992), we used an inverted confocal microscope (Nikon A1R). High-magnification images were

131   taken with a differential interference contrast 20× air (NA 0.75) objective. To visualize nuclei, DAPI

132   was excited by 405 nm laser and to visualize PNNs, Alexa488 was excited by 488 nm laser. Selected

133   areas were captured by a 20× objective in a single focal plane. Acquisition as well as processing of all

134   images was made in the same way. Image processing was carried out using Fiji software.

135   *Recording solutions for electrophysiology*

136   Unless stated otherwise, all solution chemicals were obtained from Sigma-Aldrich. The standard

137   extracellular solution contained (in mM): NaCl 137, KCl 5.0, $CaCl_2$ 1.0, $MgCl_2$ 1.2, HEPES 10, glucose

138   10, pH 7.4 (adjusted with NaOH). An alternative solution where some Na-acetate was substituted for

139   NaCl, to obtain a Cl^- concentration ($[Cl^-]_{o\_bulk}$) of 50 mM, was used in a subset of experiments aimed

140   at estimating local $[Cl^-]_o$ contributing to the driving force for Cl^-.

141   For gramicidin-perforated-patch recordings, used to estimate $[Cl^-]_i$, the standard pipette-filling

142   solution contained 300 µg ml^{-1} gramicidin (Sigma-Aldrich) and (in mM): K-acetate 140, NaCl 3.0,

143    $MgCl_2$ 1.2, HEPES 10, EGTA 1.0, pH 7.2 (adjusted with KOH). An alternative high-$[Cl^-]$ solution

144   contained 300 µg ml^{-1} gramicidin and (in mM): KCl 140, NaCl, 3.0, $MgCl_2$ 1.2, EGTA 1.0, HEPES 10, pH

145   7.2 (adjusted with KOH). The choice of pipette-filling solution was made as to facilitate detection of

146   patch rupture, with high-$[Cl^-]$ solutions being used preferentially in experiments when $[Cl^-]_i$ was

147   expected to be mainly at a low level and low-$[Cl^-]$ solutions preferentially where $[Cl^-]_i$ was expected

148   to be raised for prolonged periods. (In practice, however, this precaution was unnecessary, since

149   whenever possible rupture was suspected, this could easily be verified or disproven by controlling

150   the possibility to "set $[Cl^-]_i$" at high or low level by combined voltage control and GABA application; cf

151   the "loading procedure" described below.)

152   For conventional whole-cell recordings, used to estimate possible effects of ECM degradation on $[Cl^-$

153    $]_o$, the pipette-filling solution contained (in mM): K-acetate 125, Na-acetate 3.0, NaCl 6, $CaCl_2$ 0.9,

154   Mg-ATP 5.0, Na_2-GTP 0.4, EGTA 2.5, HEPES 10, pH 7.2 (adjusted with KOH).

155   For cell-attached recordings used to analyze the effects of presynaptic stimulation on postsynaptic

156   firing frequency, the pipette was filled with standard extracellular solution (see above).

157   A HCO_3^--buffered extracellular solution used for some control experiments (Fig. 1*D*, *E*) contained (in

158   mM): 124 NaCl, 25 $NaHCO_3$, 1.1 $NaH_2PO_4 \cdot H2O$, 3.5 KCl, 2.0 $CaCl_2$, 2.0 $MgSO_4$, 10 glucose. The solution

159   was equilibrated with a gas mixture of 95 % O_2 and 5 % CO_2.

7

160　The Cl⁻ activity coefficient was calculated using equation 3.14 given by Davies (1962) with z (valency)

161　taken to be 1. (This empiric equation is suitable for ionic strength > 0.1 M and < 0.5 M; see e. g.

162　Butler 1964; Stumm & Morgan, 1996.) For all solutions used for electrophysiology, the Cl⁻ activity

163　coefficient was 0.76; the difference between solutions being ≤ 0.6 %. The activity coefficient for Cl⁻ in

164　the complex intracellular environment during perforated-patch recording is not known, but may be

165　assumed relatively similar to that in the extracellular solution (Freedman & Hoffman, 1979;

166　Friedman, 2010). The small difference between solutions with different Cl⁻ concentrations is a

167　consequence of Cl⁻activity depending mainly on total ionic strength (Davies, 1962; Friedman, 2010)

168　and justifies the use of concentrations in the Nernst equation.

169

170　*Electrophysiological recording*

171　The general techniques and recording equipment used were as previously described (Karlsson et al.,

172　2011). Patch pipettes used had a resistance of 3.5 – 4.2 MΩ when filled with standard pipette-filling

173　solution and immersed in standard extracellular solution. The gramicidin-perforated patch method

174　(Abe et al., 1994; Kyrozis and Reichling, 1995) was used, in the majority of experiments, to avoid

175　artificial change of $[Cl^-]_i$ and ionic solutions were chosen to favour currents carried by Cl⁻ (i. e. no

176　HCO_3^-; see below). Electrophysiological recording in brain slices was performed from neurons located

177　at a depth of 50 – 150 μm, in a majority of cases 75 – 125 μm, and in no case closer to the surface or

178　bottom of the slice than 50 μm. Neurons near the center of the slice were included. Neurons with a

179　resting membrane potential ≤ –45 mV and an input resistance ≥ 100 MΩ were included. All studied

180　cells had a healthy visual appearance according to usual standards (Moyer and Brown, 2002) as

181　judged by microscopic inspection using infrared-differential interference contrast optics. The slices

182　were continuously perfused by gravity-fed extracellular solution provided by a custom-made

183　perfusion pipette positioned 100 – 200 μm from the studied cell, except for experiments with

184　presynaptic stimulation, in which the distance was 1 – 5 mm. Exchange to solution containing GABA,

8

185   glycine and/or other substances was controlled by solenoid valves via a computer. Liquid-junction

186   potentials were calculated using the Clampex software (versions 9 & 10; Molecular Devices, CA, USA)

187   and have been subtracted in all potentials given. Treatment of series resistance (R_s) between pipette

188   and cytoplasm is described below.

189   Unless stated otherwise, recording from cells in slices were made without "cleaning" (see below) and

190   with only a slight positive pressure applied to the patch pipette before sealing, just sufficient to

191   prevent clogging of the pipette tip during penetration of the tissue, with the purpose of minimal

192   effects on the structures beside the membrane patch. In a subset of cells described separately, a

193   cleaning procedure, as described by Edwards et al. (1989) was used with the purpose to

194   systematically remove the ECM covering the exposed surfaces (facing the top and sides of the slice)

195   of the cell. This implied repeated and alternated pressure and suction via a separate, large pipette

196   (tip diameter 5 – 20 μm) filled with standard extracellular solution (see above) (cf Fig 2 in Edwards et

197   al., 1989), before using a regular patch pipette for recording.

198   *Measurement of resting potential, calculation of passive [Cl⁻]ᵢ distribution and estimation of*

199   *leak conductance*. The resting potential was measured in the current-clamp mode with zero

200   command current. Similar values were obtained from the reversal potential of currents during test

201   voltage ramps (see below) without agonist in the voltage-clamp mode, when holding voltage was

202   close to the reversal potential. The $[Cl^-]_i$ expected from a passive distribution was calculated from the

203   Nernst equation using the known $[Cl^-]_o$ and with the equilibrium potential for Cl^- (E_{Cl}) set to the

204   resting potential for each individual cell. The leak conductance was estimated from the slope of a

205   linear fit to the portion of *I-V* relation around (± 5 mV) the zero current voltage during voltage ramps

206   (± 1.6 V s⁻¹) in the absence of ligands.

207   *Measurement of $E_{GABA/glycine}$ and E_{Cl} by use of voltage ramps.* The reversal potential for currents

208   evoked by GABA or glycine (E_{GABA} and $E_{glycine}$, respectively) was assumed to be described by the

209   equation $E_{GABA/glycine} = R\ T\ F^{-1} \ln \left(([Cl^-]_i + P_{rel}\ [HCO_3^-]_i)\ ([Cl^-]_o + P_{rel}\ [HCO_3^-]_o)^{-1} \right)$ where P_{rel} is HCO_3^-/Cl^-

9

210   permeability ratio of GABA or glycine receptors and R, T and F denote the gas constant, absolute

211   temperature and Faraday constant, respectively. P_{rel} was assumed to be 0.2 (Bormann et al., 1987).

212   The gramicidin pores are highly permeable to H^+ (Myers and Haydon, 1972) and thus intracellular pH

213   may be assumed equal to the pH of the pipette-filling solution. The intracellular $[HCO_3^-]$ calculated by

214   the Henderson-Hasselbalch equation with CO_2 partial pressure from Boron (2009a), solubility

215   constant and pK value, from Boron (2009b) or Kajino et al. (1982), is ~ 0.1 mM. This implies a

216   negligible effect of HCO_3^- on the reversal potential for currents through GABA$_A$ receptors (E_{GABA}) with

217   the standard HEPES-buffered extracellular solution (see above) used in most experiments, where E_{Cl}

218   = E_{GABA} = $E_{glycine}$. (In the absence of HCO_3^- in the recording pipette, E_{GABA} fits well with the Cl^-

219   equilibrium potential, E_{Cl}; Chavas and Marty, 2003).

220   The reversal potential was obtained from I-V relations constructed from currents recorded during

221   voltage ramps, given at a rate of ± 1.6 V s^{-1} (Karlsson et al., 2011). A ramp sequence consisting of

222   negative and positive voltage ramps as shown in Fig. 1A (inset) was applied twice, in the absence and

223   presence of GABA or glycine, for recording of "leak" and GABA/glycine-evoked (plus leak) currents,

224   respectively. (The timing of the second ramp was usually in the mid-50% portion of the 2-s long

225   GABA/glycine application.) Occasionally unclamped action potentials were generated during the

226   rising phase of voltage ramps in control solution without GABA/glycine. Portions of current with

227   action potentials were excluded from further analysis. The holding voltage (V_h) before, after and in-

228   between ramp sequences depended on the type of measurement: For estimation of basal $[Cl^-]_i$, V_h

229   was kept close to the resting potential. To follow recovery of $[Cl^-]_i$ after loading to high levels (see

230   below), V_h was kept close to the expected E_{Cl} (as estimated in preliminary experiments, see below),

231   to minimize Cl^- current (cf the small GABA-evoked current at holding potential, Fig. 1A). Influence on

232   $[Cl^-]_i$ was further minimized by using a symmetrical voltage ramp protocol (Yelhekar et al., 2016) (Fig.

233   1A, inset), yielding approximately similar Cl^- flux in inward and outward directions (Fig. 2A). For

234   measurement of basal $[Cl^-]_i$, special care was taken to avoid changes in $[Cl^-]_i$ during seal formation

235   between patch pipette and cell membrane: The current-clamp recording mode with I = 0 was used

10

236   during the gramicidin perforation, except for brief tests of R_s. (This implies that no current from the

237   recording pipette may change the membrane potential during the seal formation and the parallel

238   gramicidin perforation of the membrane.) In addition to these precautions, we quantified the effect

239   of the $[Cl^-]_i$-probing GABA/glycine application and voltage ramps on $[Cl^-]_i$ as described below.

240   *Procedure to minimize conductive (passive) Cl^- flux during recovery from high $[Cl^-]_i$.* To

241   minimize conductive (passive) Cl^- flux for better estimating the time course of transporter-mediated

242   changes in $[Cl^-]_i$, the holding voltage was kept as close as possible to the variable E_{Cl} during recovery

243   from high $[Cl^-]_i$. For this, an approximate time course of E_{Cl} was first obtained from test runs, with

244   initial holding voltage at an estimated (assumed) E_{Cl}: The magnitude and polarity of the first current

245   response to GABA/glycine, delivered shortly after the start of recovery period (end of GABA/glycine

246   application for loading) gave information on the magnitude and polarity of the difference between

247   estimated and true E_{Cl}. If the difference was large, the test run was aborted. If the difference was

248   small, the test run was continued with a second pair (for leak and GABA/glycine-evoked currents) of

249   ramp sequences from a new holding voltage. Again, the difference between estimated and true E_{Cl}

250   was evaluated for decision on continuation or abortion of the test run. In the absence of large

251   deviations between estimated and true E_{Cl}, the test run was continued with further ramp sequences

252   until recovery was near complete / a stable E_{Cl} was reached.

253   After a few test runs for each cell and condition, it was possible to predict the approximate time

254   course of E_{Cl} recovery, so that holding voltages reasonably close to E_{Cl} could be used. Note, however,

255   that unless the holding voltage (estimated E_{Cl}) exactly matched the true E_{Cl}, the GABA/glycine

256   application will result in some positive or negative current. It was important, therefore, to estimate

257   the influence of the GABA/glycine applications on $[Cl^-]_i$, as described below. The lack of correlation

258   between $[Cl^-]_i$ recovery time course and leak conductance (see Results) confirmed that influence of

259   passive Cl^- flux was of no major importance for the recovery.

260 *Influence of measurement procedure on [Cl⁻]ᵢ*. The influence of test pulses (with GABA or

261 glycine application) on $[Cl^-]_i$ was estimated on basis on recorded charge transfer and the estimated

262 cytosolic volume in which Cl^- equilibrates. This "equivalent volume" was obtained from the GABA-

263 evoked charge transfer during Cl^- loading (see below) and the measured rapid large change in $[Cl^-]_i$

264 between two test ramps during the loading phase. In dissociated neurons, for which cell volume is

265 easily estimated, this "equivalent volume" corresponds to about half the cell volume (Karlsson et al.,

266 2011), in good agreement with expected cytosolic volume. The charge transfer associated with a test

267 pulse of GABA during $[Cl^-]_i$ recovery was on average expected to change $[Cl^-]_i$ by 0.90 ± 0.48 mM
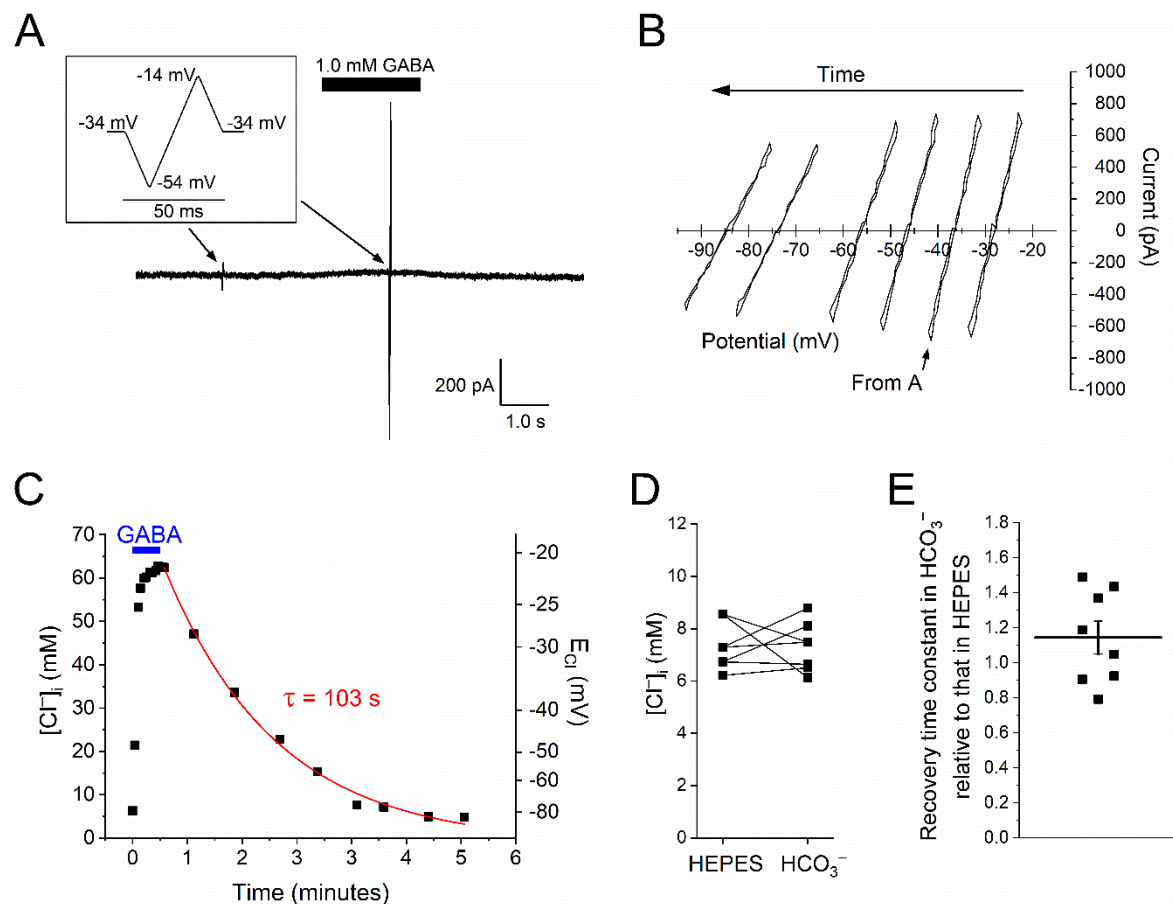
268 (mean ± SEM; 8 cells).

269

270 **Figure 1.** Principle of $[Cl^-]_i$ recovery measurement. **A**, During and after Cl^- loading, voltage ramp sequences
271 (inset) were applied in pairs, without and with GABA, from a holding voltage close to the expected E_{Cl}. Here,
272 one pair is shown, corresponding to the *I-V* relation marked "From A" in **B**. (Cf Fig. 2*A*, for similar current
273 response at a shorter time scale.) **B**, *I-V* relations obtained during $[Cl^-]_i$ recovery phase (after correction for
274 series resistance and subtraction of "leak" components; cf Fig. 2*A*). Note the shift in negative direction with
275 time. **C**, $[Cl^-]_i$ time course during loading (with 1.0 mM GABA, as indicated, at a membrane potential of ~−20

276   mV) and recovery, computed from reversal potentials (E_{GABA}). Red curve shows mono-exponential function
277   fitted to the decay, with time constant indicated. (E_{Cl} indicated to the right; note non-linear scale). **D**, Basal $[Cl^-]_i$
278   measured as described above with brain slices in a HEPES-buffered solution (left data group) and subsequently
279   after 5 - 10 min exposure to a HCO_3^--buffered solution (same cells; right data group). Cells were kept with
280   current clamped at zero to achieve resting condition, except during measurement. $[Cl^-]_i$ was calculated from
281   the reversal potential of the GABA-evoked current as described in the main text. The difference between the
282   two solutions was not significant (p = 0.61, paired Wilcoxon signed rank test). **E**, Ratio between $[Cl^-]_i$ recovery
283   time constants (measured as in **C**) with a HEPES-buffered extracellular solution and with a HCO_3^--buffered
284   solution, in the same cells. The ratio is not significantly different from 1 (p = 0.31, one sample Wilcoxon signed
285   rank test).

286

287   *Loading cells with Cl^-*. Loading cells to a high $[Cl^-]_i$, for enabling subsequent estimates of Cl^-

288   transport capacity, was made by combining a depolarized holding voltage (~ –20 - 0 mV) with

289   application of 1.0 mM GABA (Sigma-Aldrich) or 1.0 mM glycine (Sigma-Aldrich) for 20 - 30 s (Karlsson

290   et al., 2011). A single voltage-ramp sequence, applied before the agonist, was then used to estimate

291   leak currents for repeated $[Cl^-]_i$-probing voltage ramps during this long-lasting agonist application (cf

292   Fig. 2A-C in Yelhekar et al. 2017).

293   *Subtraction of leak and capacitive currents*. The *I-V* relation for "leak" currents induced by the

294   voltage ramps in the absence of ligands for Cl^- permeable channels was (after correction for R_s

295   effects as described below) often well fitted by a linear function. In some cases, especially at

296   relatively positive voltages, a slightly curved relation was obtained, likely due to some contribution of

297   voltage-sensitive currents. In the latter cases, the *I-V* relation was well fitted by the exponential

298   function: $I = A + B\, e^{V/C}$ (A, B and C being constants). The obtained "leak" *I-V* relation was used to

299   calculate and subtract leak (and small voltage-gated) current components from the current

300   measured in the presence of GABA or glycine during short ligand application (Karlsson et al., 2011;

301   Yelhekar et al., 2017). The use of the mathematically expressed relation between leak current and R_s-

302   corrected voltage rather than the current directly recorded during the voltage ramps (in the absence

303   of GABA/glycine) provides a better estimate of leak current during voltage ramps in the presence of

304   GABA/glycine, since the voltage with and without agonist as a rule differs as a consequence of the

305   induced currents across the series resistance (R_s).

13

306   The current during the rising as well as declining phases of the voltage ramp sequence (Fig. 1*A*, inset)

307   was used for the *I-V* relation (apparently seen as two superimposed curves, e.g. Fig. 1*B*). Often, the

308   reversal potential from the rising and declining phases of the ramp sequence were not significantly

309   different (Fig. 1*B*; see also Fig. 2*A*, right), but in some cases a contribution of capacitive current

310   (which is constant but of opposite sign during rising and declining phases) caused a slight offset of

311   the two curves. In the latter cases, E_{Cl} (or E_{GABA} or $E_{glycine}$) was obtained from the midpoint (mean)

312   between the two reversal potentials. $[Cl^-]_i$ or $[Cl^-]_o$, depending on the experiment, was subsequently

313   calculated from the relation between reversal potential and $[Cl^-]$ given above (for E_{Cl}, Nernst

314   equation). As previously described (Karlsson et al., 2011), $GABA_B$ receptors do not contribute

315   significantly to GABA-evoked currents in the studied neurons.

316   *Series resistance compensation*. Online series resistance (R_s) compensation during electrical

317   recording was not used since it is usually accompanied by additional noise and since full

318   compensation is not possible with maintained electrical stability (see e.g. The Axon Guide.

319   Electrophysiology & Biophysics Laboratory Techniques", 3rd ed., 2012, Molecular Devices, CA, U.S.A.).

320   To better account for effects of R_s, all voltages were corrected offline by subtracting $R_s\,I$, where *I* is

321   raw recorded current and R_s the series resistance as measured by the "membrane test" procedure in

322   the Clampex software. The above description of leak and capacitive current subtraction explains how

323   the different effects of R_s on membrane voltage during recording of leak currents compared with

324   agonist-induced currents were taken into account. Series resistance in the gramicidin-perforated

325   patch mode was 37 ± 2 MΩ (n = 110) and in the whole-cell mode 23 ± 2 MΩ (n = 25). For recording of

326   voltage-gated Ca^{2+} currents in amphotericin-perforated patch mode, see below.

327   *Whole-cell recording for estimation of E_{Cl}*. The whole-cell recording mode was used in some

328   experiments to dialyze the cytoplasm with a known Cl^- concentration and enable estimation of the

329     $[Cl^-]_o$ that contributes to E_{Cl}, and reveal a hypothetical difference from $[Cl^-]$ in the external bulk

330   solution as suggested by Glykys et al. (2014a). In these experiments we used Cs^+ rather than K^+ as the

14

331   major cation in the pipette, to reduce background noise, to improve voltage-clamp control (Chen et

332   al., 1999) and to reduce Cl^- transport by KCC2 (Cs^+ competing with other cations; inhibition constant

333   9.7 mM; Williams and Payne, 2004). In the whole-cell mode, equilibration of Cl^- between pipette and

334   cytosol is expected within a few seconds for spherical cells (Pusch and Neher, 1988), but deviations

335   of $[Cl^-]_i$ from $[Cl^-]_{pip}$ may possibly arise as a consequence of influence of dendrites or Cl^- leak across

336   the membrane (or across pipette-membrane seal). Such influence was here suggested by the

337   correlation between leak conductance and measured E_{Cl} (and thus calculated $[Cl^-]_o$) when high $[Cl^-]$

338   was present in the external bulk solution (Fig. 2*D*, upper two lines). With reduced $[Cl^-]$ in the external

339   bulk solution, however, the observed data (Fig. 2*D*, lower two lines) did not reveal any significant

340   influence of such leak.

341   *Amphotericin B-perforated recording of Ca^{2+} currents*. Whole-cell Ca^{2+} currents were recorded

342   in the amphotericin B-perforated patch configuration (120 µg ml^{-1} amphotericin B; Sigma-Aldrich)

343   under voltage-clamp conditions, with voltage-gated Na^+ currents blocked by 2.0 µM tetrodotoxin

344   (Latoxan) in the extracellular solution and voltage-gated K^+ currents blocked or reduced by Cs^+

345   substituted for K^+ in the pipette solution. Currents were activated by voltage steps from –54 mV to –

346   14 mV. The leak currents and capacitive currents were subtracted using scaled current responses to

347   negative potential steps. The finding of linear *I-V* relations for currents evoked in preoptic neurons in

348   response to voltage steps in the range –40 to –140 mV justified this procedure (Sundgren-Andersson

349   and Johansson, 1998). Series resistance compensation was not used for these recordings and

350   maximum voltage error (at peak current) was estimated to 15 mV. (Series resistance in the

351   amphotericin-perforated patch mode was 25 ± 2 MΩ; n = 19.) Further, only the relative components

352   of Ca^{2+} current amplitudes and charge transfer in each cell were used for analysis, to account for

353   intercellular variability in absolute Ca^{2+} currents.

354   *Presynaptic stimulation.* Extracellular stimulation of presynaptic nerve fibers was made as

355   previously described (Malinina et al., 2005). Postsynaptic responses to such stimulation were

15

356   recorded in the cell-attached mode (10 – 18 cells, depending on type of experiment) and verified in

357   the gramicidin-perforated patch mode (see above; 3 – 4 cells for each type of experiment). Effects on

358   firing frequency were analyzed with data pooled from the two used recording configurations.

359   All electrical recordings were performed at room temperature (21 – 23 °C).

360

361 *Protein estimation*

362 Brain slices from the medial preoptic area (as described above) were used for protein estimation by

363 Western blot (see below). From each animal, a maximum of three adjacent brain slices were used,

364 and divided along the midline to achieve a maximum of six hemispheric slices for separate exposure

365 to different test substances or use as control. The choice of (left or right) hemispheric slice for the

366 different exposures was made at random to avoid any systematic inter-hemispheric differences. The

367 protein samples obtained from the brain tissue was split and run repeatedly (three times each, with

368 average taken, for improved reliability) on separate gels.

369 *Estimation of total KCC2 protein and of αII-spectrin fragments.* For total protein extraction, the

370 brain slices were homogenized in RIPA buffer (Thermo Fisher) containing a protease inhibitor cocktail

371 (Sigma-Aldrich). In experiments for αII-spectrin degradation, 1.0 % of each phosphatase inhibitor

372 cocktail 2 and 3 (Sigma-Aldrich) as well as EDTA and EGTA (5.0 mM each; Sigma-Aldrich) were added

373 to prevent additional lysis-induced Ca^{2+} dependent calpain activation. Non-soluble proteins were

374 separated by centrifugation at 13 000 g for 10 min at 4 °C. The protein concentration of individual

375 samples was measured using the BCA protein assay kit (Thermo Fisher). Protein samples (8 – 12 μg;

376 30 μg for αII-spectrin degradation assessment) in reducing (5.0 % 2-mercaptoethanol) sample buffer

377 (Bio-Rad) were heated at 70° for 30 or 10 (for αII-spectrin) min and loaded on precast 4 – 12 %

378 polyacrylamide gels (Bio-Rad) or on homemade 8 % gels (for αII-spectrin) and separated by SDS-PAGE

379 electrophoresis. Subsequently, proteins were transferred to polyvinylidene difluoride (PVDF)

380 membranes (Thermo Fisher) in freshly prepared buffer containing 25 mM Tris-base, 192 mM glycine

381 and 20 % (v/v) methanol. Non-specific antibody binding was blocked by 5.0 % blotting-grade blocker

382 non-fat dry milk (Bio-Rad) in Tris-buffered saline (TBS) and tween 20 (0.1 %) for 1 h at room

383 temperature. Membranes were incubated with primary antibodies in 5.0 % non-fat dry milk-

384 containing TBS-tween solution. Primary antibodies, anti-KCC2 (1: 5000; Millipore), anti-transferrin

385 receptor (1:500; Invitrogen), anti-α-fodrin (1:5000; Enzo, clone AA6) and anti-β-tubulin (1:10000;

17

386   Abcam) were used to stain KCC2, transferrin receptor, αII-spectrin (full form and fragments) and β-

387   tubulin respectively. After overnight incubation with primary antibodies, membranes were incubated

388   with horseradish peroxidase (HRP)-linked anti-mouse (1:5000; GE Healthcare) or HRP-linked anti-

389   rabbit (1:1000; Cell signaling) secondary antibodies at room temperature for 1 h. Chemiluminescent

390   detection was done using Luminata Forte Western HRP substrate (Millipore) and images were taken

391   on an Odyssey Fc imaging system (LI-COR). Quantification of chemiluminescent signals was made

392   using Image studio (version 3.1, LI-COR). Protein levels of KCC2, transferrin receptor and αII-spectrin

393   (full form and fragments) were estimated relative to the level of β-tubulin.

394   *Estimation of KCC2 dimer and monomer levels in membrane fraction.* ChABC- or vehicle-

395   treated brain slices (as described above) were homogenized in lysis buffer containing 50 mM Tris·HCl,

396   pH 7.4, 1.0 mM EDTA, supplemented with 1.0 % CLAP (chymostatin (Sigma-Aldrich), leupeptin

397   hemisulfate, antipain-dihydrochloride, pepstatin A (Carl Roth)), 0.5 mM phenylmethyl sulphonyl

398   fluoride (PMSF; Carl Roth), 1.0 % each phosphatase inhibitor cocktails 2 and 3 (Sigma-Aldrich), and 25

399   mM iodoacetamide (Sigma-Aldrich), used to block free thiol groups and prevent ex-vivo KCC2

400   multimerization (Blaesse et al., 2006; Mahadevan et al., 2014). To isolate membrane proteins from

401   cytosolic ones, homogenized samples were centrifuged at 10 000 g for 30 min. The obtained pellet

402   was resuspended in CHAPS buffer (50 mM Tris·HCl, pH 7.4, 10 mM CHAPS (Glycon Biochemicals),

403   0.05 mM EDTA) containing CLAP, PMSF, phosphatase inhibitor cocktails 2 and 3 and iodoacetamide

404   in concentrations as above and allowed to solubilize for 3 h on a rotating platform at 4 °C. The

405   samples were centrifuged for 1 h at 10 000 g and the supernatants were recovered. Cleared lysates

406   (10 μg) were suspended in non-reducing electrophoresis sample buffer (6.0 % SDS, 20 % glycerol,

407   62.5 mM Tris·HCl, pH 6.8, 0.01 % bromophenol blue) to prevent disassembly of KCC2 oligomers,

408   which are sensitive to sulfhydryl-reducing agents but resistant to SDS (Blaesse et al., 2006).

409   Subsequently, the proteins were separated by SDS-PAGE on 7.5 % gels and immunoblotted with anti-

410   KCC2 (1:1000) and anti-calnexin antibody (1:2000; Enzo Life Sciences). Densitometric analysis of

411 corresponding bands was performed by Image Studio software (LI-COR Biosciences). KCC2 protein

412 level in the membrane fraction was estimated relative to the level of the membrane protein calnexin.

413 *Experimental design and statistical analysis.*

414 Statistical analysis was performed using OriginPro, versions 9.0 – 2019. All data are presented as

415 mean ± SEM unless otherwise stated. Effects were evaluated by the non-parametric one-sample

416 Wilcoxon test, paired Wilcoxon signed rank test or Mann-Whitney test, as indicated. Spearman´s

417 rank correlation coefficient was used to evaluate possible correlations between measured variables

418 or recording parameters. For electrophysiological experiments, including estimates of Cl^-

419 concentrations, numbers (n) given denote the number of cells studied, with paired tests used for

420 comparison of different conditions for the same cell. The cells used to analyse each test

421 (substance/condition) were obtained from a minimum of five (and up to 22) brain slices from a

422 minimum of four (and up to 19) rats. For Western blot data, numbers (n) denote the number of

423 animals studied, with paired tests used to compare differently treated brain tissue from right and left

424 hemispheres of the same individual. P-values < 0.05 were taken to indicate significant differences.

425

Results

427 **The low basal $[Cl^-]_i$ depends on KCC2 as well as on the ECM**

428 We estimated basal $[Cl^-]_i$ in preoptic neurons in slice preparations of rat brain, by direct recording of

429 Cl^- currents through $GABA_A$- or glycine-receptors during voltage ramps (Karlsson et al., 2011) (Fig.

430 2*A*). The gramicidin-perforated patch method (Abe et al., 1994; Kyrozis and Reichling, 1995) was used

431 to avoid artificial change of $[Cl^-]_i$ and ionic solutions were chosen to favour currents carried by Cl^- (i.

432 e. no HCO_3^-; see Materials and Methods). In control conditions, $[Cl^-]_i$ was significantly lower than

433 expected from a passive distribution (7.0 ± 0.5 mM vs 10.2 ± 0.5 mM; n = 13, p = 0.0024, paired

19

434 Wilcoxon signed rank test; Fig. 2*B*). Such a difference is expected as a consequence of KCC2-mediated

435 transport, with the effect on $[Cl^-]_i$ depending on the membrane Cl^- conductance (Johansson et al.,

436 2016). Here, the selective KCC2-antagonist VU0255011-1 (10 μM for 30 min) increased $[Cl^-]_i$ to 18.4 ±

437 2.6 mM (n = 9, p = 1.7 10^{-5}, Mann-Whitney test; Fig. 2*C*) without affecting the resting potential

438 (control: −69 ± 3 mV, n = 13; VU0255011-1: −68 ± 3 mV, n = 9; p = 0.59, Mann-Whitney test between

439 groups), showing that KCC2 is critically required for the low basal $[Cl^-]_i$.

440

441
442
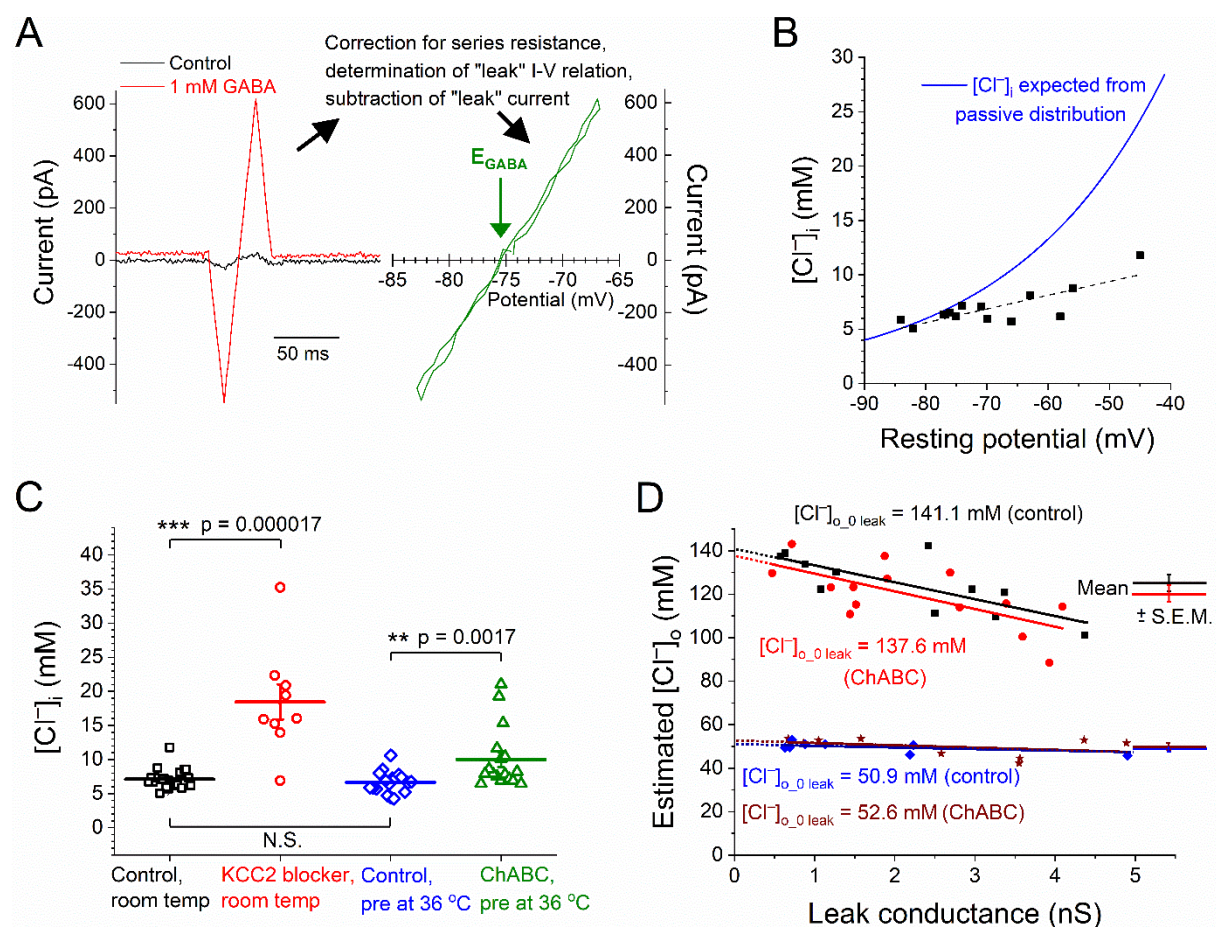
Figure 2. Basal $[Cl^-]_i$ depends on KCC2 and on the ECM, but $[Cl^-]_o$ does not depend on the ECM. **A**, Raw currents (left) in response to voltage ramps (−74 to −94 to −54 to −74 mV) in the absence or presence of GABA, showing principle of measurement. *I-V* curve (right) gives E_{Cl} (= E_{GABA}). **B**, Basal $[Cl^-]_i$ versus resting potential (dashed line: linear fit) in comparison with $[Cl^-]_i$ computed for passive distribution (blue line). **C**, Significant effects of KCC2 antagonist and of pre-treatment with ChABC on $[Cl^-]_i$. **D**, Estimated $[Cl^-]_o$ versus leak conductance, with nominal bulk $[Cl^-]_o$ of 146.4 mM (upper two lines and symbol sets) or 50 mM (lower two lines and symbol sets). Lines: linear fits, dotted extrapolation to zero leak conductance with corresponding $[Cl^-]_{o\_0\ leak}$ indicated. Horizontal lines and error bars (in **C** and **D**, right) denote mean ± S.E.M.
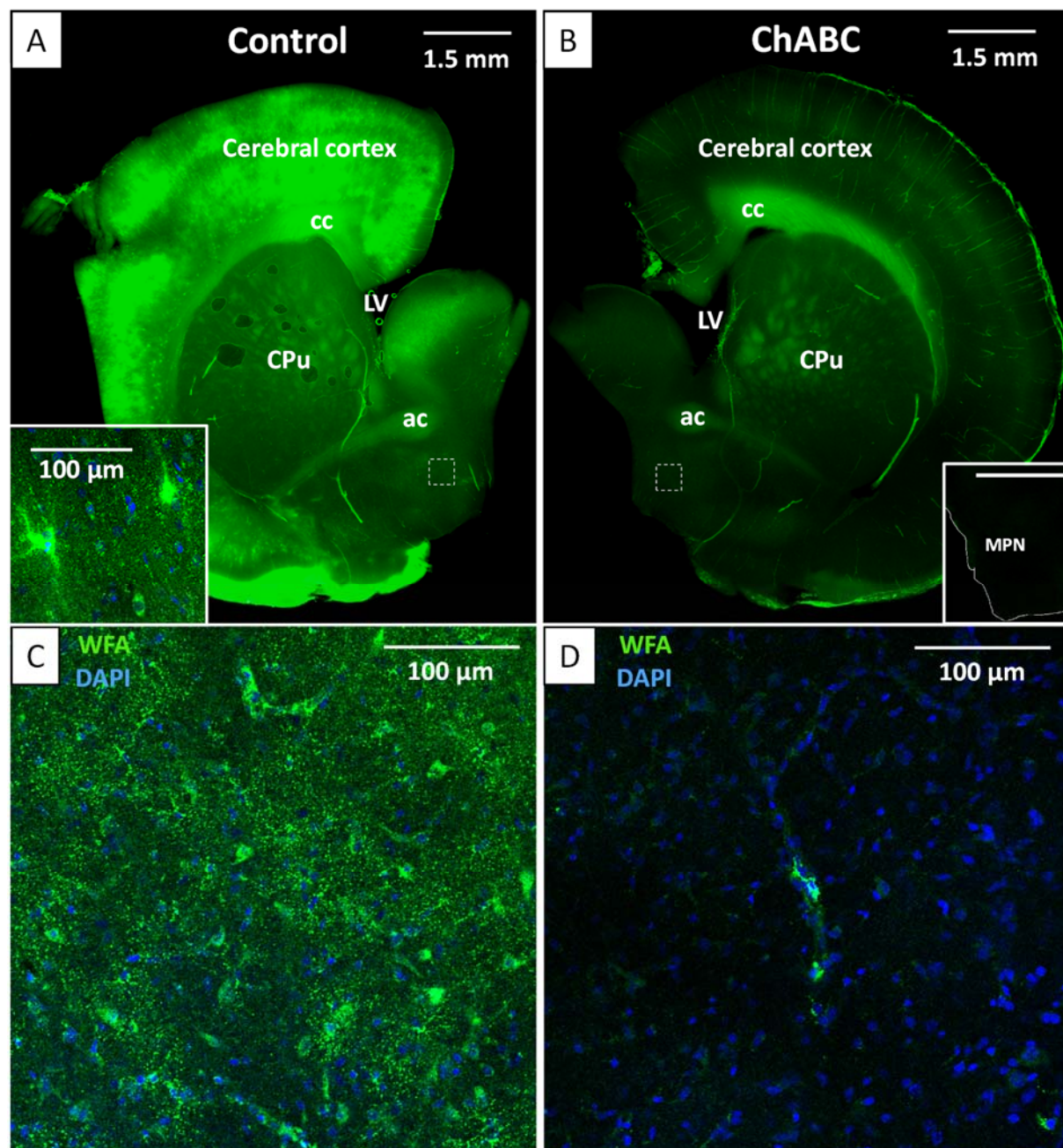
451

Figure 3. ChABC treatment degrades ECM. *A*, *B*, Low-magnification images of hemispheral coronal brain slices incubated for 2 h in vehicle (0.1 % BSA, Control, *A*) or ChABC (0.2 U ml^{-1}, *B*) and stained with *Wisteria floribunda* agglutinin (WFA) to label chondroitin sulphate proteoglycans present in the ECM. Dashed white boxes denote the approximate location of the medial preoptic nucleus (MPN) shown at higher magnification below (*C*, *D*). Note, that the WFA signal is much weaker in the slice treated with ChABC as compared with the control. Inset in *A* shows a confocal image from neocortex (control), obtained with 20× objective, with typical WFA-positive perineuronal nets surrounding some cells. Inset in *B* shows an area including the MPN from a negative control slice, incubated without WFA (scale bar 1.5 mm as in *A*; thin white line drawn to show border of slice). *C*, *D*, Confocal images obtained with 20× objective; control (*C*) and ChABC treated (*D*) medial preoptic area; merged WFA (green) and DAPI (blue; for DNA in cell nuclei) staining. cc – corpus callsosum, ac – anterior commissure, CPu – caudate putamen (striatum), LV – lateral ventricle.

465 We next examined if the ECM is important for the basal $[Cl^-]_i$. Chondroitinase ABC treatment (0.2 U

466 ml^{-1}; see Materials and Methods) resulted in ECM degradation, as verified histochemically by WFA

467 staining (Fig. 3). In parallel, basal $[Cl^-]_i$ increased from 6.6 ± 0.4 mM (n = 18) to 10.0 ± 1.1 mM (n = 17,

468 p = 1.7 10^{-3}, Mann-Whitney test; Fig. 2*C*). Basal $[Cl^-]_i$ did not significantly depend on whether a

469 HEPES- or bicarbonate-buffered extracellular solution was used (Fig. 1*D*). The resting potential did

470 not differ significantly (Mann-Whitney test, p = 0.30) between control cells (−70 ± 2 mV, n = 19;

471 exposed to the same temperature as ChABC-treated cells) and those exposed to ChABC (−67 ± 2 mV,

472 n = 20).

473

474 **ECM degradation does not affect local $[Cl^-]_o$**

475 According to Glykys et al. (2014a), ChABC increases $[Cl^-]_i$ as a consequence of removed ECM charges

476 and the associated increase in local $[Cl^-]_o$. However, the idea that local extracellular charges would

477 alter the driving force for Cl^- across the cell membrane has been questioned on basis of

478 thermodynamic principles (Kaila et al., 2014; Voipio et al., 2014) and such effects may possibly occur

479 only if there is a local displacement of Cl^- in the immediate vicinity of the Cl^--permeable channels

480 (Savtchenko et al., 2017). To experimentally verify that the driving force for Cl^- is not affected by ECM

481 charges, we estimated whether the $[Cl^-]_o$ contributing to the driving force for Cl^-, possibly different

482 from the Cl^- concentration in the external bulk solution ($[Cl^-]_{o\_bulk}$), was affected by ECM degradation.

483 Therefore, we used the whole-cell patch-clamp mode to dialyze the cell with a known Cl^-

484 concentration (7.8 mM), which enabled estimation of $[Cl^-]_o$ from E_{GABA}, obtained with voltage ramps

485 as above, and from the defined $[Cl^-]_i$. In these experiments, Cs^+ was substituting K^+ as major cation in

486 the pipette, to reduce KCC2-mediated transport (Williams and Payne, 2004; see Materials and

487 Methods). With $[Cl^-]_{o\_bulk}$ = 146.4 mM, the estimated $[Cl^-]_o$ was 125 ± 4 mM (n = 11), substantially

488 less than $[Cl^-]_{o\_bulk}$. However, the method may be influenced by Cl^- leak into the cell, as suggested by

489 a negative correlation between membrane leak conductance and estimated $[Cl^-]_o$ (Fig. 2*D*, black). To

490   improve the estimation, we extrapolated $[Cl^-]_o$ linearly to zero leak, thus obtaining $[Cl^-]_o$ = 141.1 mM,

491   i. e. relatively close to $[Cl^-]_{o\_bulk}$. We next tested the hypothesis that ChABC treatment is accompanied

492   by increased $[Cl^-]_o$. Mean $[Cl^-]_o$ after ChABC treatment was 120 ± 4 mM (n = 14) (Fig. 2*D*, red), not

493   significantly different from control (Mann-Whitney test), and the improved $[Cl^-]_o$ estimate obtained

494   by extrapolation to zero leak was 137.6 mM. We also estimated $[Cl^-]_o$ when $[Cl^-]_{o\_bulk}$ was 50 mM and

495   less Cl^- leak into the cell was expected. In this case, mean $[Cl^-]_o$ was within 1.0 mM from the expected

496   value, in control conditions (49.1 ± 0.9 mM; n = 9; Fig. 2*D*, blue) as well as after ChABC treatment

497   (49.9 ± 1.4 mM; n = 9; Fig. 2*D*, wine). Again, there was no significant difference between control and

498   ChABC-treated cells (Mann-Whitney test). The lack of change in measured E_{GABA} and estimated $[Cl^-]_o$

499   contradicts the idea that ChABC increases the driving force by increasing local $[Cl^-]_o$ and thus also

500   contradicts the idea that such effects would be the cause for increased $[Cl^-]_i$ after ChABC treatment.

501

502   **KCC2-mediated $[Cl^-]_i$ recovery rate depends on ECM integrity**

503   From the above results, it seems likely that KCC2 function depends on ECM integrity. To test this

504   hypothesis, we first estimated Cl^- transport rate from repeated measurements of $[Cl^-]_i$ during

505   recovery after loading to $[Cl^-]_i$ ~40 - 75 mM (see Materials and Methods and Fig. 1; cf Yelhekar et al.,

506   2017). The recovery showed an exponential time course (time constant 111 ± 14 s; n = 19) and was

507   not significantly altered by the NKCC1-antagonist bumetanide (10 µM; Sigma-Aldrich; Fig. 4*A;* n = 8,

508   paired Wilcoxon signed rank test), but was dramatically slowed down by VU0255011-1 (10 µM; Fig.

509   4*A*, *B*). After 14 minutes of recovery, estimated $[Cl^-]_i$ was 5.3 ± 0.3 mM in control solution, but 41.5 ±

510   2.3 mM in the presence of VU0255011-1 (p = 7.8 10^{-3}, paired Wilcoxon signed rank test; Fig. 4*B*),

511   suggesting a main role of KCC2 for $[Cl^-]_i$ recovery. In similarity with basal $[Cl^-]_i$, the $[Cl^-]_i$ recovery time

512   constant did not significantly depend on whether a HEPES- or bicarbonate-buffered extracellular

513   solution was used (Fig. 1*E*). We subsequently tested the hypothesis that the ECM is important not

514   only for basal $[Cl^-]_i$, but also for the rate of KCC2-mediated Cl^- transport. The $[Cl^-]_i$ recovery time

23

515   constant, after Cl$^-$- loading cells in control slices pre-incubated at ~ 36 $^\circ$C for 2 h (to enable

516   comparison with ChABC-treated slices), was 137 ± 18 s (n = 19), not statistically different (Mann-

517   Whitney test) from that in control slices kept at room temperature (21 – 23 $^\circ$C). (Note that even

518   when pre-incubation at 36 $^\circ$C was used, evaluation of [Cl$^-$]$_i$ recovery time constant was made at room

519   temperature.) However, ChABC treatment dramatically increased the [Cl$^-$]$_i$ recovery time constant to

520   441 ± 84 s (n = 15, p = 4.8 10^{-6}, Mann-Whitney test; Fig. *4C*, *D*), confirming that the ECM is important

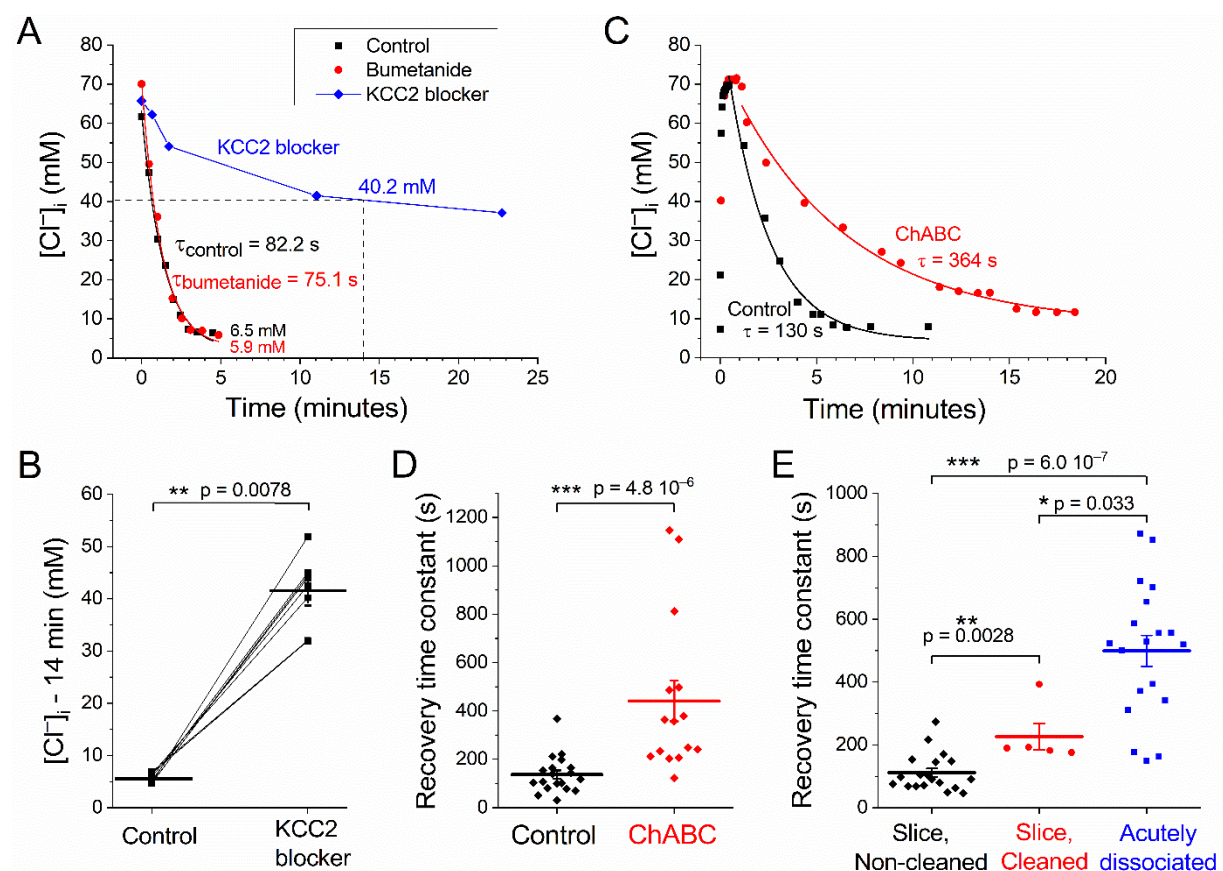521   for the rate of KCC2-mediated Cl$^-$ transport.

522

Figure 4. Cl$^-$ extrusion rate depends on KCC2 and on the ECM. *A*, Time course of [Cl$^-$]$_i$ recovery after load to ~70 mM. Single neuron in control solution, with bumetanide (10 µM) and with VU0255011-1 (10 µM). Solid lines: exponential fits (control and bumetanide), linear interpolation (KCC2 antagonist). *B*, [Cl$^-$]$_i$ after nominally 14 minutes recovery (see below; cf dashed lines in *A*); control and with 10 µM VU0255011-1 (paired data from 8 neurons). *C*, [Cl$^-$]$_i$ recovery time course after pre-incubation for 2 h at 35-37 $^\circ$C in the absence (Control) or presence of ChABC. *D*, Significant effect of ChABC on [Cl$^-$]$_i$ recovery time constants (cf *C*). *E*, Significant effect of cell cleaning and of dissociation on [Cl$^-$]$_i$ recovery time constants (cf *A* and *C*). Data for acutely dissociated cells from Yelhekar et al. (2017). Horizontal lines and error bars (in *B*, *D* and *E*) denote mean ± S.E.M. The [Cl$^-$]$_i$ at a nominal time point of 14 min in *B* was estimated by extrapolation of the near-steady [Cl$^-$]$_i$ in cases where [Cl$^-$]$_i$ decayed to < 10 mM within 10 minutes and by linear interpolation of [Cl$^-$]$_i$ at an interval where [Cl$^-$]$_i$ changed less than ~1 mM/min in cases with slower decay, as illustrated by dashed lines in *A*.

534 As an alternative to ChABC treatment, we used the "cleaning" method for patch-clamp recording in

535 slices (Edwards et al., 1989; see Materials and Methods), with a stream of saline to remove the ECM

536 covering the top and other exposed surfaces of neuronal soma and basal neurites. This type of

537 cleaning is, like attenuation of ECM with β-D-xyloside, a procedure that facilitates giga-seal formation

538 at patch-clamp recording (Izu and Sachs, 1991). $[Cl^-]_i$ recovery in cleaned cells was much slower than

539 in control conditions (time constant 227 ± 42 s; n = 5, cleaned, vs 111 ± 14, control, n = 19, p =

540 0.0028, Mann-Whitney test; Fig. 4*E*). Thus, the two independent tests, with different procedures to

541 affect the ECM, suggest a role of the ECM in controlling the rate of Cl^- extrusion. $[Cl^-]_i$ recovery

542 measured previously with similar methods in acutely dissociated preoptic neuronal cell bodies,

543 where we expect even less ECM, is still slower (499 ± 49 s, n = 19; Yelhekar et al., 2017; comparison

544 with present control values: p = $6.0 \ 10^{-7}$, Mann-Whitney test), further strengthening this idea (Fig.

545 4*E*).

546 The resting membrane properties of the cleaned cells in slices and those of the acutely dissociated

547 cells differed somewhat from those reported for non-cleaned cells in slices reported above. Thus, the

548 resting potential was –62 ± 6 mV (n = 5) and –60 ± 3 mV (n = 19) for cleaned and for dissociated cells,

549 respectively. The corresponding values for leak conductance was 2.0 ± 0.3 nS (cleaned) and 0.91 ±

550 0.15 nS (dissociated) and for membrane capacitance 11 ± 1 pF (cleaned) and 5.5 ± 0.3 pF

551 (dissociated) in the same cell groups. (Series resistance did not differ significantly between any of the

552 studied cell groups). A correlation analysis performed on the two large cell groups (non-cleaned in

553 slices, n = 19 and acutely dissociated, n = 19), however, showed that the time constant of recovery

554 from high $[Cl^-]_i$ was neither significantly correlated to the membrane capacitance nor to leak

555 conductance or resting potential when studied within each preparation (i. e. Spearman´s rank

556 correlation coefficient was not significantly different from zero.) Thus, differences in resting

557 membrane properties *per se* are unlikely to account for the differences in time course of $[Cl^-]_i$

558 recovery. The lack of correlation between $[Cl^-]_i$ recovery and leak conductance is in agreement with

25

559   the experimental design where contribution of passive Cl⁻ flux is minimized by keeping the

560   membrane voltage close to E_{Cl}.

561   A summary of ChABC effects on neuronal properties is shown in Table 1. A correlation analysis

562   showed that that neither resting potential, leak conductance, membrane capacitance, resting $[Cl^-]_i$,

563   nor $[Cl^-]_i$ recovery time constant were significantly correlated with the series resistance. (As

564   expected, leak conductance was strongly positively correlated with membrane capacitance:

565   Spearman's rank correlation coefficient 0.681, p = 0.0013.)

566

	Control	n	ChABC	n	p / N.S.
U_{rest}	−70 ± 2 mV	19	−67 ± 2 mV	20	N.S.
g_{leak}	1.5 ± 0.1 nS	19	1.3 ± 0.2 nS	18	N.S.
C_m	17.6 ± 1.8 pF	21	15.1 ± 2.2 pF	19	N.S.
$[Cl^-]_{i\_rest}$	6.6 ± 0.4 mM	18	10.0 ± 1.1 mM	17	$1.7 \cdot 10^{-3}$
$\tau_{recovery}$	137 ± 18 s	19	441 ± 84 s	15	$4.8 \cdot 10^{-6}$

571 **Table 1.** Summary of main resting neuronal properties, $[Cl^-]_i$ recovery time constant and the effect of ChABC
572 treatment on those properties. The far right column gives p-values from a Mann-Whitney test for difference
573 between control conditions and ChABC treatment. Note that only resting $[Cl^-]_i$ and $[Cl^-]_i$ recovery time constant
574 were significantly affected. The control values reported were obtained from cells pre-incubated at at ~ 36 ℃ for
575 2 h to enable comparison with cells from ChABC-treated slices. N.S., not significant; U_{rest}, resting potential; g_{leak},
576 leak conductance; C_m, membrane capacitance; $[Cl^-]_{i\_rest}$, resting $[Cl^-]_i$; $\tau_{recovery}$, $[Cl^-]_i$ recovery time constant.

577

578 **ECM degradation is accompanied by calpain-mediated reduction of KCC2 protein**

579   Next, we used Western blot analysis to test whether the dependence of KCC2 function and of $[Cl^-]_i$

580   on the ECM is mediated by an altered amount of KCC2 protein. Indeed, ChABC significantly reduced

581   the total level of KCC2 protein (to 73 ± 8 %; n = 13, p = 0.0081) but did not significantly affect the

582   level of transferrin receptor (p = 0.57, n = 12), another membrane protein (Fig. 5*A*). Since KCC2

583   function may depend on the amount of di- or oligomers in the membrane (Blaesse et al., 2006;

584   Watanabe et al., 2009), we also tested the hypothesis that ChABC differentially affects KCC2

585   monomers and dimers. ChABC significantly reduced the amount of KCC2 monomers (to 56 ± 7 %; n =

586   12, p = 9.8 10^{-4}) but the slight apparent reduction (to 84 ± 10 %; n = 12) of dimers was not significant

587   (p = 0.13; Fig. 5*B*), suggesting that the monomeric form is of functional importance for Cl$^-$ transport

588   sensitive to ChABC.

589   KCC2 may be cleaved by calpain, a Ca^{2+}-dependent protease which has been linked to synaptic

590   plasticity and neurodegeneration (Baudry et al., 2013), likely as a consequence of Ca^{2+} influx through

591   NMDA receptors (Chamma et al., 2013; Puskarjov et al., 2012). Therefore, we tested the hypothesis

592   that the effect of ECM removal on KCC2 protein level is mediated by calpain activity. In the presence

593   of the calpain-inhibitor calpeptin (30 µM; Sigma-Aldrich), ChABC failed to reduce the KCC2 level (Fig.

594   5*C*; p = 1.0), suggesting that ECM removal triggers calpain-dependent cleavage of KCC2.

595

596   **KCC2 downregulation is mediated by Ca^{2+} influx through N-type channels**

597   The KCC2 level was dramatically increased (to 263 ± 37 %; n = 8, p = 0.0078) in the presence of the

598   NMDA-receptor blocker MK-801 (1.0 µM; Sigma-Aldrich) when compared with control (Fig. 5*C*),

599   implying a role for NMDA receptors in maintaining the basal KCC2 level. However, ChABC significantly

600   reduced the KCC2 level (by 35 ± 10 %; n = 8; p = 0.023) also in the presence of MK-801, contradicting

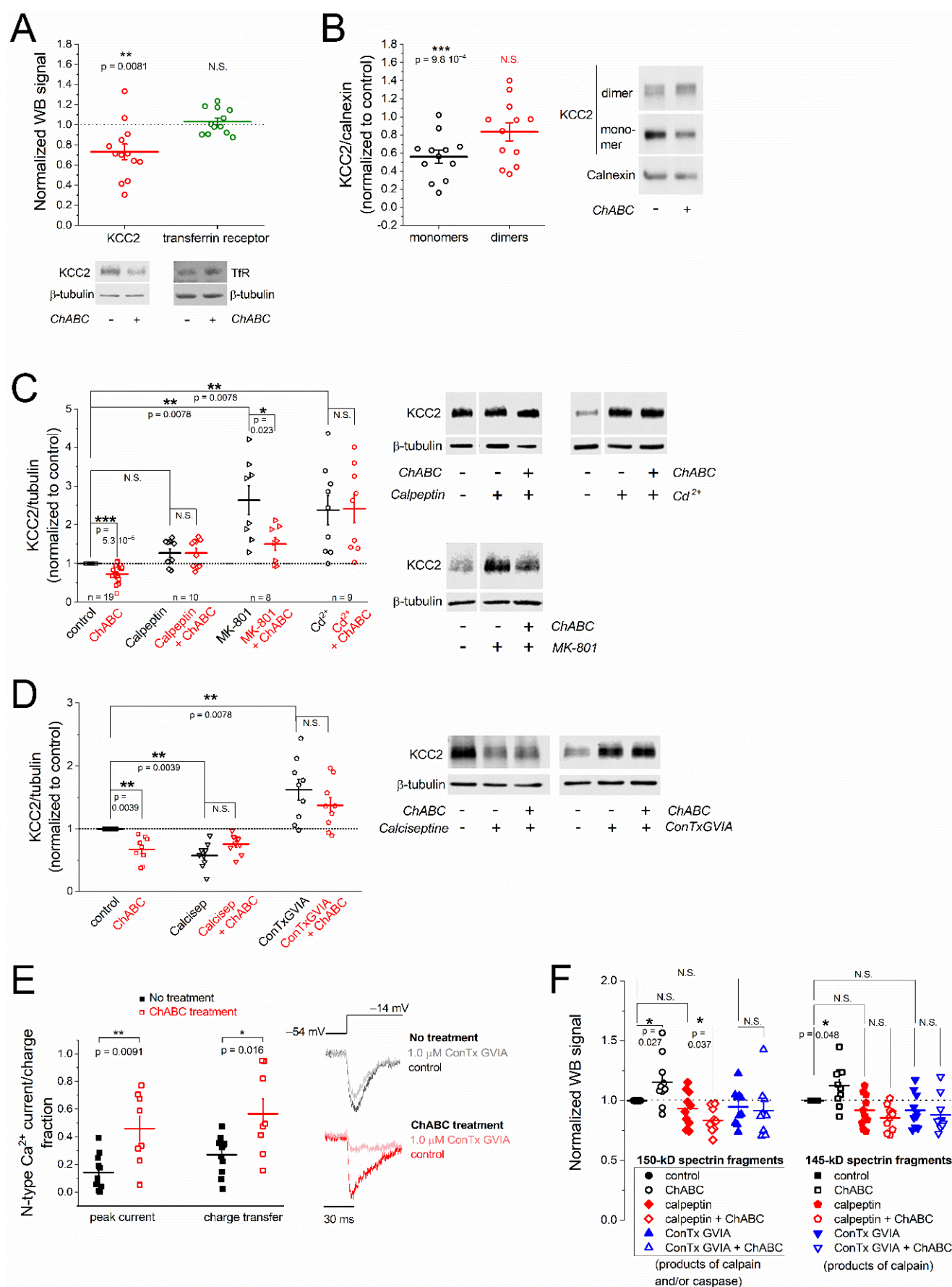601   the hypothesis that ECM degradation affects KCC2 via Ca^{2+} influx through NMDA receptors.

Figure 5. KCC2 protein level depends on the ECM, calpain and Ca²⁺ channels.

602

603

28

604 *(Legend to Fig. 5, continued)*

605 ***A***, Top: Effect of ChABC treatment on KCC2 and transferrin-receptor (TfR) protein levels relative to β-tubulin (β-
606 tub) in whole-cell lysate. Data normalized to control. (WB: Western blot.) Bottom: representative WB. ***B***, Left:
607 Effect of ChABC treatment on KCC2 monomer and dimer levels in membrane fraction, relative to calnexin.
608 Right: representative WB. ***C – D***, Left: Effects of calpeptin (30 μM), MK-801 (1.0 μM) and Cd^{2+} (200 μM) (***C***) and
609 of calciseptine (Calcisep; 500 nM) and ω-conotoxin GVIA (ConTxGVIA; 1.0 μM) (***D***) on the KCC2 protein level in
610 whole-cell lysate in the presence or absence of ChABC, estimated as in ***A***. Right: representative WB. ***E***, ChABC
611 effects on N-type Ca^{2+} channels. Current contributed by N-type Ca^{2+} channels, estimated as ω-conotoxin GVIA-
612 sensitive fraction of peak Ca^{2+} current (left two symbol sets) and of charge transfer (right two symbol sets),
613 during the first 100 ms after command voltage steps from −54 mV to −14 mV. Control conditions (filled
614 symbols) and after ChABC treatment (similar as for protein analysis; open symbols). Example raw current traces
615 during voltage step (top) shown in the right panel. To enable comparison between cells with different Ca^{2+}
616 current magnitudes, only relative, ω-conotoxin GVIA-sensitive, current and charge fractions were used in the
617 analysis of ChABC effects. Note that significantly larger fractions of current and charge transfer are sensitive to
618 ω-conotoxin GVIA after ChABC treatment. ***F***, ChABC effects on αII-spectrin degradation. Normalized (to control)
619 WB signals for 150 kD (left) and 145 kD (right) fragments of αII-spectrin in whole-cell lysate in control
620 conditions and after treatment with ChABC, calpeptin, ω-conotoxin GVIA (ConTx GVIA) and combinations of
621 ChABC and calpeptin/ConTx GVIA as indicated. Levels of αII-spectrin are relative to β-tubulin. Bars indicate
622 mean ± S.E.M. Statistical significance was evaluated with the paired Wilcoxon signed rank test.

623

624

625 Another possible source of Ca^{2+} influx, that hypothetically may trigger calpain activation upon ECM

626 degradation, is voltage-gated Ca^{2+} channels. This idea was supported by the findings that in the

627 presence of the high-threshold Ca^{2+}-channel blocker Cd^{2+} (200 μM) (Sundgren-Andersson and

628 Johansson, 1998), the level of KCC2 was markedly increased (to 238 ± 38 %; n = 9, p = 0.0078)

629 compared with control, and not significantly (p = 0.65, n = 9) affected by ChABC (Fig. 5*C*). To identify

630 the involved channel types, the effect of ChABC treatment on the level of KCC2 was studied in the

631 presence of calciseptine (500 nM; Latoxan) and ω-conotoxin GVIA (1.0 μM; Alomone labs), selective

632 blockers of L- and N-type voltage-gated Ca^{2+} channels, respectively. Surprisingly, incubation in

633 calciseptine *per se* significantly *reduced* KCC2 (by 42 ± 7 %; n = 9, p = 0.0039), to a level similar to that

634 in ChABC alone (p = 0.57) and also similar to the KCC2 level in a combination of ChABC and

635 calciseptine (p = 0.098; Fig. 5*D*). The effect of calciseptine suggests that Ca^{2+} entry via L-type channels

636 is not coupled to the KCC2 reduction via calpain but on the contrary contributes to KCC2

637 upregulation. ω-conotoxin GVIA, however, induced an opposite effect, significantly increasing the

638 KCC2 level (to 162 ± 16 %; n = 9, p = 0.0078) when incubated without ChABC. Importantly, when co-

639   applied with ω-conotoxin GVIA, ChABC did not significantly reduce the KCC2 level below that in ω-

640   conotoxin GVIA alone (p = 0.50; Fig. 5*D*). This suggests that Ca^{2+} influx through N-type channels does

641   contribute to the KCC2 downregulation upon ECM degradation.

642   Whole-cell Ca^{2+} currents recorded under voltage-clamp conditions (see Materials and Methods)

643   confirmed that the ω-conotoxin GVIA-sensitive, presumably N-type channel-mediated, fraction of

644   high-voltage activated Ca^{2+} current was significantly larger after treatment with ChABC (Fig. 5*E*).

645   Thus, the ω-conotoxin GVIA-sensitive fraction contributed 14 ± 4 % of the peak current in control

646   conditions but increased to 46 ± 9 % after ChABC treatment (p = 0.0091, control: n = 11, ChABC: n =

647   8, Mann-Whitney test) and the corresponding charge transfer (during 100 ms) increased from 27 ± 4

648   % to 57 ± 11 % (p = 0.016, Mann-Whitney test).

649   The results above suggest that the ChABC-induced reduction of KCC2 protein level is mediated via

650   calpain as a consequence of Ca^{2+} influx through N-type channels. To confirm that ChABC treatment

651   activates calpain, we analyzed the effect of ChABC on αII-spectrin degradation, commonly used as

652   indicator of calpain activation (Wang, 2000), by Western blot. Spectrin fragments of 150 kDa,

653   products of calpain or caspase-3 activity, 145 kDa, products of calpain activity, and 120 kDa, products

654   of caspase-3 activity (Nath et al., 1996), were detected in control tissue and were neither significantly

655   affected by tissue exposure to calpeptin (n = 10) nor by exposure to ω-conotoxin GVIA (n = 10). After

656   treatment with ChABC, the levels of 150 and 145 kDa fragments, but not that of 120 kDa fragments,

657   were significantly increased (n = 10, Fig. 5*F*), as expected from ChABC-induced calpain activation. This

658   increase was blocked by calpeptin (n = 10, Fig. 5*F*), confirming that it was caused by calpain activity.

659   The ChABC-induced increase of 150 and 145 kDa spectrin fragments was also blocked by ω-conotoxin

660   GVIA (n = 10, Fig. 5*F*), confirming the requirement of N-type Ca^{2+} channels for the activation of

661   calpain.

662

663

30

ECM degradation may turn GABA effect from inhibition into excitation

Finally, we tested the hypothesis that the effects of ECM degradation on KCC2 function and on $[Cl^-]_i$ are relevant for $GABA_A$-receptor mediated transmission. In control slices, presynaptic stimulation was followed by inhibition of spontaneously firing cells (Fig. 6*A,* top trace). This inhibition was abolished by the $GABA_A$-receptor antagonist gabazine (SR-95531, Tocris; n = 8, Fig. 6*A*, lower trace). In ChABC-treated slices, spontaneous firing frequency was, neither before nor after (0 – 40 ms) stimulation, significantly different from control. A sequence of high-frequency stimulation (HFS; 500 stimuli at 40 Hz), however, significantly reduced the inhibitory effect of 0.4-Hz stimulation in ChABC-treated cells (n = 22, p = 0.0061, paired Wilcoxon signed ranks test), but not in control cells (n = 13, p = 0.20, paired Wilcoxon signed rank test; Fig. 6*B*). Ten minutes after HFS, the change was accentuated and an initial excitatory effect (Fig. 6*C*) was seen in several ChABC-exposed cells upon 0.4-Hz stimulation, resulting in average excitation in ChABC-exposed cells (Fig. 6*D*), but average inhibition in control cells (Fig. 6*D*) 0 – 40 ms after stimulation. The reduction in immediate post-HFS synaptic inhibition of ChABC-exposed cells (Fig. 6*B*, middle) was abolished (p = 0.45, n = 18, paired Wilcoxon signed ranks test) when the calpain blocker calpeptin (30 μM) was present during slice incubation with ChABC (Fig. 6*B*, right), and synaptic inhibition 10 minutes after HFS was rescued (Fig. 6*D*, right; p = 0.27, n = 18, paired Wilcoxon signed ranks test). These effects of calpeptin on synaptic transmission are consistent with our biochemical analysis of KCC2 and calpain activity and imply that calpain transduces attenuation of ECM into degradation of KCC2 and thereby increases $[Cl^-]_i$ and modifies GABA-mediated transmission.
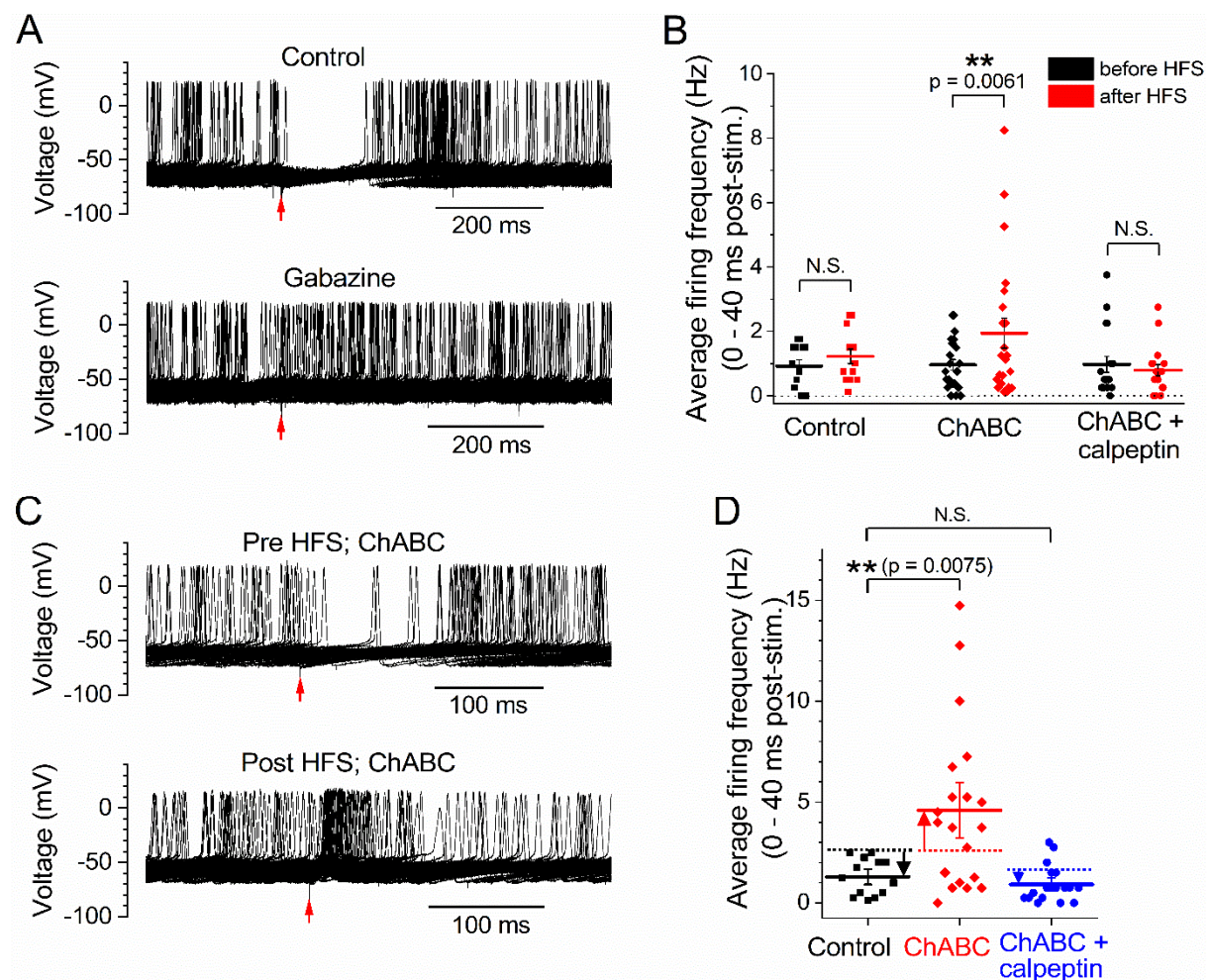
31

Figure 6. Synaptic transmission after high-frequency stimulation is altered by ECM degradation. *A*, Presynaptic stimulation (arrow) at 0.4 Hz in the presence of glutamate-receptor blockers (20 µM NBQX + 50 µM APV) inhibits spontaneous firing (top; 100 superimposed traces). After addition of the GABA$_A$-receptor antagonist gabazine (SR-95531; 3.0 µM), similar stimulation does not inhibit spontaneous firing (bottom; 100 superimposed traces). *B*, A period of high-frequency stimulation (HFS; 500 stimuli at 40 Hz) does not change the inhibitory effect of 0.4-Hz stimulation on firing frequency in cells from control slices (left) but reduces the inhibitory effect in cells from ChABC-treated slices (middle). This effect of ChABC is abolished by the calpain inhibitor calpeptin (30 µM; right). (Horizontal lines and error bars: mean ± S.E.M.) *C*, Top: Hundred superimposed traces showing initial inhibitory effect of 0.4-Hz stimulation (arrow) on a cell in a ChABC-treated slice. Bottom: Excitatory effect of similar stimulation in the same cell but 10 minutes after HFS (500 stimuli at 40 Hz). *D*, Ten minutes after HFS, the change in transmission is accentuated in many ChABC-exposed cells, and frequently the initial inhibition (left) has changed to excitation (middle). Calpeptin (30 µM) prevents the loss of inhibition in ChABC-treated slices (right). Data show impulse frequency 0 – 40 ms after stimulus (repeated at 0.4 Hz). Solid horizontal lines and error bars: mean ± S.E.M. Dotted lines show pre-stimulation mean frequency; arrows indicate the change to mean post-stimulus (0 – 40 ms) frequency, downward for inhibition (control and ChABC + calpeptin) and upward for excitation (ChABC).

Discussion

707

708 In conclusion, the present study verifies the recently suggested importance of the ECM for neuronal

709 Cl^- homeostasis (Glykys et al., 2014a) and uncovers a novel molecular mechanism for control of

710 GABA-mediated transmission. Direct electrophysiological measurement showed that basal $[Cl^-]_i$ is

711 lower than expected for a passive distribution and depends on KCC2 and on ECM integrity. However,

712 the results are not consistent with the debated mechanism involving a strong effect of ECM negative

713 charges on $[Cl^-]_o$ and $[Cl^-]_i$ (Glykys et al., 2014a). Thus, ECM degradation does not affect $[Cl^-]_o$, but

714 affects KCC2, mainly in monomeric form, and basal $[Cl^-]_i$. Importantly, the rate of KCC2-mediated Cl^-

715 extrusion after a high load, critical to neural coding (Doyon et al., 2016), also depends on ECM

716 integrity. The mechanism by which the ECM degradation influences KCC2 function, largely depending

717 on the Ca^{2+}-activated protease calpain, partly overlaps with that for the glutamate-evoked reduction

718 in KCC2 associated with interictal-like activity (Chamma et al., 2013; Puskarjov et al., 2012). However,

719 our results do not support a role of NMDA-receptors in the effect of ECM removal. Rather, they

720 suggest that ECM degradation reduces KCC2 level via Ca^{2+} entry through N-type Ca^{2+} channels and

721 subsequent calpain activation. A role for calpain in increasing excitability via reduced KCC2 and

722 increased $[Cl^-]_i$ is particularly intriguing since calpain is activated at brain injury and during

723 epileptogenesis (Lam et al., 2017). The present findings therefore suggest a positive feedback

724 mechanism by which epileptogenesis may be self-sustaining, with seizure-induced calpain activation

725 contributing to further increased cell excitability.

726 Our findings also indicate a novel differential and opposing regulation of KCC2 via different Ca^{2+}

727 channel subtypes. The suggested upregulation of KCC2 level via Ca^{2+} entry through L-type channels is

728 consistent with the roles of L-type channels and Ca^{2+}/calmodulin-dependent protein kinase II for

729 elevation of KCC2 transcription (Li et al., 2016) and of KCC2 protein level (Liedtke et al., 2013). Since

730 removal of the major ECM component hyaluronic acid reduces Ca^{2+} influx through L-type channels in

731 hippocampal CA1 cells (Kochlamazashvili et al., 2010), this may provide a calpain-independent

33

732   mechanism by which the ECM regulates KCC2. In principle, the N-type channel- and calpain-

733   dependent pathway and the L-type channel-dependent, calpain-independent pathway may act in

734   concert to reduce the KCC2 level upon ECM degradation, but apparently the former pathway

735   dominates the effect of ChABC studied here.

736   Finally, the present results show that the ECM is critically important for synaptic function, since ECM

737   degradation may change a dominant inhibitory effect to excitatory. Similar changes in excitability

738   have been described for other conditions with intracellular Cl^- accumulation (Cohen et al., 2002;

739   Coull et al., 2003; Khazipov et al., 2015). We speculate that in conditions, such as epilepsy, where the

740   ECM may be downregulated (Soleman et al., 2013), effects on $[Cl^-]_i$ may contribute to the pathology.

741   Furthermore, enzymatic degradation of ECM has been shown to re-open a "window" of enhanced

742   developmental plasticity and aided functional recovery in regeneration, stroke and amblyopia

743   (Soleman et al., 2013) and calpain inhibition ameliorates seizure burden in an epilepsy model (Lam et

744   al., 2017). Further studies are warranted to explore the possibility that these therapeutic effects at

745   least partially are mediated by $[Cl^-]_i$-dependent changes in GABAergic transmission.

Conclusions

747   In this work, we show that degradation of the extracellular matrix (ECM) which surrounds brain cells

748   increases basal $[Cl^-]_i$, and reduces the rate of Cl^- extrusion via a reduced amount of the Cl^-

749   transporting protein K-Cl-cotransporter 2 (KCC2). This results in a reduced inhibitory, or even an

750   excitatory, effect of GABA-mediated transmission. The findings imply a novel pathway for the control

751   of neuronal $[Cl^-]_i$ and excitability and may explain how degradation of ECM may re-open a window for

752   developmental forms of neuroplasticity in the adult central nervous system.

753

Acknowledgements

759

References

761   Abe Y, Furukawa K, Itoyama Y, Akaike N (1994) Glycine response in acutely dissociated ventromedial

762   hypothalamic neuron of the rat: new approach with gramicidin perforated patch-clamp

763   technique. J Neurophysiol 72:1530–1537.

764   Baudry M, Chou MM, Bi X (2013) Targeting calpain in synaptic plasticity. Expert Opin Ther Targets

765   17:579–592.

766   Ben-Ari Y (2014) The GABA excitatory/inhibitory developmental sequence: a personal journey.

767   Neuroscience 279:187–219. doi:10.1016/j.neuroscience.2014.08.001

768   Ben-Ari Y (2002) Excitatory actions of GABA during development: the nature of the nurture. Nat Rev

769   Neurosci 3:728–739.

770   Blaesse P, Guillemin I, Schindler J, Schweizer M, Delpire E, Khiroug L, Friauf E, Nothwang HG (2006)

771   Oligomerization of KCC2 correlates with development of inhibitory neurotransmission. J

772   Neurosci 26:10407–10419.

773   Bormann J, Hamill OP, Sakmann B (1987) Mechanism of anion permeation through channels gated by

774   glycine and gamma-aminobutyric acid in mouse cultured spinal neurones. J Physiol 385:243–

775   286.

776   Boron WF (2009a) Organization of the respiratory system. In: Medical physiology (Boron WF,

777   Boulpaep EL, eds), pp613-629. Philadelphia: Saunders, Elsevier.

778   Boron WF (2009b) Acid-base physiology. In: Medical physiology (Boron WF, Boulpaep EL, eds),

779   pp652-671. Philadelphia: Saunders, Elsevier.

780   Bukalo O, Schachner M, Dityatev A (2001) Modification of extracellular matrix by enzymatic removal

781   of chondroitin sulfate and by lack of tenascin-R differentially affects several forms of synaptic

782   plasticity in the hippocampus. Neuroscience 104:359-369.

783   Butler JN (1964) Ionic equilibration. A mathematical approach. Reading, Massachusetts: Addison-

784   Wesley.

785   Chamma I, Heubl M, Chevy Q, Renner M, Moutkine I, Eugène E, Poncer JC, Lévi S (2013) Activity-

786   dependent regulation of the K/Cl transporter KCC2 membrane diffusion, clustering, and

787   function in hippocampal neurons. J Neurosci 33:15488–15503.

788   Chavas J, Marty A (2003) Coexistence of excitatory and inhibitory GABA synapses in the cerebellar

789   interneuron network. J Neurosci 23:2019–2031.

790   Chen H-X, Otmakhov N, Lisman J (1999) Requirements for LTP Induction by pairing in hippocampal

791   CA1 pyramidal cells. J Neurophysiol 82:526–532.

792   Cho C-H (2014) Star players sidelined in chloride homeostasis in neurons. Front Cell Neurosci 8:114.

793   doi:10.3389/fncel.2014.00114

794   Choi HJ, Lee CJ, Schroeder A, Kim YS, Jung SH, Kim JS, Kim DY, Son EJ, Han HC, Hong SK, Colwell CS,

795   Kim YI (2008) Excitatory actions of GABA in the suprachiasmatic nucleus. J Neurosci 28:5450–

796   5459.

797   Cohen I, Navarro V, Clemenceau S, Baulac M, Miles R (2002) On the origin of interictal activity in

798   human temporal lobe epilepsy in vitro. Science 298:1418–1421.

799   Coull JAM, Boudreau D, Bachand K, Prescott SA, Nault F, Sík A, De Koninck P, De Koninck Y (2003)

800   Trans-synaptic shift in anion gradient in spinal lamina I neurons as a mechanism of neuropathic

801   pain. Nature 424:938–942.

802   Davies CW (1962) Ion Association. London: Butterworths.

803   DeFazio RA, Heger S, Ojeda SR, Moenter SM (2002) Activation of A-type gamma-aminobutyric acid

804   receptors excites gonadotropin-releasing hormone neurons. Mol Endocrinol 16:2872–2891.

805   Delpire E, Staley KJ (2014) Novel determinants of the neuronal Cl⁻ concentration. J Physiol 592:4099–

806   4114.

807   Doyon N, Prescott SA, De Koninck Y (2016) Mild KCC2 hypofunction causes inconspicuous chloride

808   dysregulation that degrades neural coding. Front Cell Neurosci 9. doi:10.3389/fncel.2015.00516

809   Edwards FA, Konnerth A, Sakmann B, Takahashi T (1989) A thin slice preparation for patch clamp

810   recordings from neurones of the mammalian central nervous system. Pflügers Arch 414:600–

811   612.

812   Freedman JC, Hoffman JF (1979) Ionic and osmotic equilibria of human red blood cells treated with

813   nystatin. J Gen Physiol 74:157-185.

814   Friedman MH (2010) Principles and models of biological transport, 2nd ed. New York: Springer.

815   Glykys J, Dzhala V, Egawa K, Balena T, Saponjian Y, Kuchibhotla KV, Bacskai BJ, Kahle KT, Zeuthen T,

816   Staley KJ (2014a) Local impermeant anions establish the neuronal chloride concentration.

817   Science 343:670–675.

818   Glykys J, Dzhala V, Egawa K, Balena T, Saponjian Y, Kuchibhotla KV, Bacskai BJ, Kahle KT, Zeuthen T,

819   Staley KJ (2014b) Response to comments on "Local impermeant anions establish the neuronal

820   chloride concentration". Science 345:1130.

821   Haam J, Popescu IR, Morton LA, Halmos KC, Teruyama R, Ueta Y, Tasker JG (2012) GABA is excitatory

822   in adult vasopressinergic neuroendocrine cells. J Neurosci 32:572–582.

823   Härtig W, Brauer K, Brückner G (1992) Wisteria floribunda agglutinin-labelled nets surround

824   parvalbumin-containing neurons. Neuroreport 3:869–872.

825   Howell MD, Bailey LA, Cozart MA, Gannon BM, Gottschall PE (2015) Hippocampal administration of

826   chondroitinase ABC increases plaque-adjacent synaptic marker and diminishes amyloid burden

827   in aged APPswe/PS1dE9 mice. Acta Neuropathol Commun 3:54. doi:10.1186/s40478-015-0233-

828   z

829   Huberfeld G, Wittner L, Clemenceau S, Baulac M, Kaila K, Miles R, Rivera C (2007) Perturbed chloride

830   homeostasis and GABAergic signaling in human temporal lobe epilepsy. J Neurosci 27:9866–

831   9873.

832   Hughes DI, Bannister AP, Pawelzik H, Thomson AM (2000) Double immunofluorescence, peroxidase

833   labelling and ultrastructural analysis of interneurones following prolonged electrophysiological

834   recordings in vitro. J Neurosci Methods 101:107-116.

835   Izu YC, Sachs F (1991) Inhibiting synthesis of extracellular matrix improves patch clamp seal

836   formation. Pflügers Arch 419:218–220.

837   Johansson S, Yelhekar TD, Druzin M (2016) Commentary: Chloride regulation: a dynamic equilibrium

838   crucial for synaptic inhibition. Front Cell Neurosci 10. doi:10.3389/fncel.2016.00182

839   Kaila K, Price TJ, Payne JA, Puskarjov M, Voipio J (2014) Cation-chloride cotransporters in neuronal

840   development, plasticity and disease. Nat Rev Neurosci 15:637–654.

841   Kajino K, Matsumura Y, Fujimoto M (1982) [Determination of dissociation exponent of CO2 used in

842   Henderson-Hasselbalch equation by means of bicarbonate-selective microelectrode]. Nihon

843   Seirigaku Zasshi. 44:663–673.

844   Karlsson U, Druzin M, Johansson S (2011) Cl^- concentration changes and desensitization of $GABA_A$

845   and glycine receptors. J Gen Physiol 138:609–626. doi:10.1085/jgp.201110674

846   Khazipov R, Valeeva G, Khalilov I (2015) Depolarizing GABA and developmental epilepsies. CNS

847   Neurosci Ther 21:83–91.

848   Kochlamazashvili G, Henneberger C, Bukalo O, Dvoretskova E, Senkov O, Lievens PM-J, Westenbroek

849   R, Engel AK, Catterall WA, Rusakov DA, Schachner M, Dityatev A (2010) The extracellular matrix

850   molecule hyaluronic acid regulates hippocampal synaptic plasticity by modulating postsynaptic

851   L-type Ca^{2+} channels. Neuron 67:116–128.

852   Kyrozis A, Reichling DB (1995) Perforated-patch recording with gramicidin avoids artifactual changes

853   in intracellular chloride concentration. J Neurosci Methods 57:27–35.

854   Lam PM, Carlsen J, González MI (2017) A calpain inhibitor ameliorates seizure burden in an

855   experimental model of temporal lobe epilepsy. Neurobiol Dis 102:1-10.

856   Li B, Tadross MR, Tsien RW (2016) Sequential ionic and conformational signaling by calcium channels

857   drives neuronal gene expression. Science 351:863–867.

858   Liedtke W, Yeo M, Zhang H, Wang Y, Gignac M, Miller S, Berglund K, Liu J (2013) Highly conductive

859   carbon nanotube matrix accelerates developmental chloride extrusion in central nervous

860   system neurons by increased expression of chloride transporter KCC2. Small 9:1066–1075.

861   Luhmann HJ, Kirischuk S, Kilb W (2014) Comment on "Local impermeant anions establish the

862   neuronal chloride concentration". Science 345:1130.

863   Mahadevan V, Pressey JC, Acton BA, Uvarov P, Huang MY, Chevrier J, Puchalski A, Li CM, Ivakine EA,

864   Airaksinen MS, Delpire E, McInnes RR, Woodin MA (2014) Kainate receptors coexist in a

865   functional complex with KCC2 and regulate chloride homeostasis in hippocampal neurons. Cell

866   Rep 7:1762–1770.

867   Malinina E, Druzin M, Johansson S (2005) Fast neurotransmission in the rat medial preoptic nucleus.

868   Brain Res 1040:157–168.

869   Morita S, Oohira A, Miyata S (2010) Activity-dependent remodeling of chondroitin sulfate

870   proteoglycans extracellular matrix in the hypothalamo-neurohypophysial system. Neuroscience

871   166:1068–1082.

872   Moyer JR, Brown TH (2002) Patch-clamp techniques applied to brain slices. In: Neuromethods 35:

873   Patch-clamp analysis: Advanced techniques (Walz W, Boulton AA, Baker GB, eds), pp 135-193.

874   Totowa, New Jersey: Humana.

875   Myers VB, Haydon DA (1972) Ion transfer across lipid membranes in the presence of gramicidin A. II.

876   The ion selectivity. Biochim Biophys Acta 274:313–322.

877   Nath R, Raser KJ, Stafford D, Hajimohammadreza I, Posner A, Allen H, Talanian RV, Yuen P, Gilbertsen

878   RB, Wang KKW (1996) Non-erythroid α-spectrin breakdown by calpain and interleukin 1β-

879   converting-enzyme-like protease(s) in apoptoti cells: contributory roles of both protease

880   families in neuronal apoptosis. Biochem J 319:683-690.

881   Pusch M, Neher E (1988) Rates of diffusional exchange between small cells and a measuring patch

882   pipette. Pflügers Arch 411:204–211.

883   Puskarjov M, Ahmad F, Kaila K, Blaesse P (2012) Activity-dependent cleavage of the K-Cl

884   cotransporter KCC2 mediated by calcium-activated protease calpain. J Neurosci 32:11356–

885   11364.

886   Savtchenko LP, Poo MM, Rusakov DM (2017) Electrodiffusion phenomena in neuroscience: a

887   neglected companion. Nat Rev Neurosci 18:598-612.

888   Senkov O, Andjus P, Radenovic L, Soriano E, Dityatev A (2014) Neural ECM molecules in synaptic

889   plasticity, learning, and memory. Prog Brain Res 214:53-80.

890   Soleman S, Filippov MA, Dityatev A, Fawcett JW (2013) Targeting the neural extracellular matrix in

891   neurological disorders. Neuroscience 253:194–213.

892   Stumm W, Morgan JJ (1996) Aquatic chemistry: Chemical equilibria and rates in natural waters. 3rd

893   ed. New York: John Wiley & Sons.

894   Sundgren-Andersson AK, Johansson S (1998) Calcium spikes and calcium currents in neurons from

895   the medial preoptic nucleus of rat. Brain Res 783:194–209.

896   Voipio J, Boron WF, Jones SW, Hopfer U, Payne JA, Kaila K (2014) Comment on "Local impermeant

897   anions establish the neuronal chloride concentration". Science 345:1130.

898   Wang KKW (2000) Calpain and caspase: can you tell the difference? Trends Neurosci 23:20-26.

899   Watanabe M, Wake H, Moorhouse AJ, Nabekura J (2009) Clustering of neuronal K^+-Cl^- cotransporters

900   in lipid rafts by tyrosine phosphorylation. J Biol Chem 284:27980–27988.

901   Williams JR, Payne JA (2004) Cation transport by the neuronal K^+-Cl^- cotransporter KCC2:

902   thermodynamics and kinetics of alternate transport modes. Am J Physiol Cell Physiol 287:C919–

903   C931.

904   Yelhekar TD, Druzin M, Karlsson U, Blomqvist E, Johansson S (2016) How to properly measure a

905   current-voltage relation?—Interpolation vs. ramp methods applied to Studies of $GABA_A$

906   receptors. Front Cell Neurosci 10. doi:10.3389/fncel.2016.00010

907   Yelhekar TD, Druzin M, Johansson S (2017) Contribution of resting conductance, $GABA_A$-receptor

908   mediated miniature synaptic currents and neurosteroid to chloride homeostasis in central

909   neurons. eNeuro 4:e0019-17.2017. doi: 10.1523/ENEURO.0019-17.2017